Astronomy & Astrophysics manuscript no. output
July 10, 2026

The role of accretion efficiency, natal kicks, and angular momentum transport in the formation of the *Gaia* black holes

Michela Mapelli ⋆[1,2,3,4], Cecilia Sgalletta[1,2], Johanna Müller-Horn[5,6], Giuliano Iorio[7], Stefano Rinaldi[1,2], Christian Burt[1,2], Daniel Marín Pina[1,2], Amedeo Romagnolo[1,2,3]

[1]Universität Heidelberg, Zentrum für Astronomie (ZAH), Institut für Theoretische Astrophysik, Albert-Ueberle-Str. 2, 69120, Heidelberg, Germany
[2]Universität Heidelberg, Interdisziplinäres Zentrum für Wissenschaftliches Rechnen, Heidelberg, Germany
[3]Physics and Astronomy Department Galileo Galilei, University of Padova, Vicolo dell'Osservatorio 3, I–35122, Padova, Italy
[4]INAF - Osservatorio Astronomico di Padova, Vicolo dell'Osservatorio 5, I-35122, Padova, Italy
[5]Max-Planck-Institut für Astronomie, Königstuhl 17, 69117 Heidelberg, Germany
[6]Fakultät für Physik und Astronomie, Universität Heidelberg, Im Neuenheimer Feld 226, 69120 Heidelberg, Germany
[7]Departament de Física Quàntica i Astrofísica, Institut de Ciències del Cosmos, Universitat de Barcelona, Martí i Franquès 1, E-08028 Barcelona, Spain

Received XXX / Accepted YYY

ABSTRACT

Gaia has the potential to deliver several tens of new dormant black holes (BHs) with low-mass stellar companions (hereafter, *Gaia* BHs) in the upcoming fourth data release. Three *Gaia* BHs are already known, but their formation pathways remain uncertain. Here, we perform a large parametric study to explore the formation of *Gaia* BHs from isolated binary systems with the population-synthesis code SEVN and compare our models with the properties of the three already reported *Gaia* BHs. Specifically, we explore the impact of accretion efficiency, mass transfer stability, natal kicks, angular momentum transport, and core-collapse supernova prescriptions. We find that models in which stable mass transfer is highly non-conservative and angular momentum is lost as a wind from the donor surface (Jeans mode) maximize the probability of forming dormant systems that match the properties of the observed *Gaia* BHs in terms of both orbital period and eccentricity, because such assumptions prevent the initial orbit from shrinking too much when the BH progenitor fills its Roche lobe. If we allow for common-envelope evolution, we find that models with common-envelope ejection efficiency $\alpha < 1$ predict dormant systems with orbital periods that are too short compared to the observed *Gaia* BHs. The eccentricity of the observed *Gaia* BHs, when combined with information about orbital period and BH mass, favors relatively large natal kicks, similar to those inferred from Galactic neutron stars. Finally, models in which BH natal kicks are low – e.g. because they are modulated by fallback – result in the formation of a large population of dormant BHs with long orbital periods ($P_{\rm orb} > 10^4$ days), which will be tested soon by the fourth *Gaia* data release.

Key words. stars: black holes – stars: binaries – black hole physics – methods: numerical

1. Introduction

Dormant black holes (BHs; i.e., X-ray-silent BHs that are members of a binary system with a companion star; Zeldovich & Guseynov 1966; Trimble & Thorne 1969) represent a unique opportunity for understanding the fate of massive stars and provide complementary information to gravitational wave events (Abbott et al. 2016; Abac et al. 2025a,b) and X-ray systems (Özel et al. 2010; Farr et al. 2011). The number of known dormant BHs is steadily increasing through radial velocity measurements and astrometry. Dedicated spectroscopic surveys have searched for dormant BHs in globular clusters, resulting in a still -debated candidate in the Large Magellanic Cloud cluster, NGC1850 (Saracino et al. 2022, 2023; El-Badry & Burdge 2022), and two dormant BHs and one additional candidate in the Milky Way cluster, NGC3201 (Giesers et al. 2018, 2019). All these systems are associated with relatively low-mass black holes ($4 - 10$ $M_\odot$) and low-mass companion stars ($0.5 - 1$ $M_\odot$), and the orbital periods and eccentricities span a wide range of values: from a few days to several hundred days for the former, and from nearly zero to more than 0.6 for the latter.

The two known dormant BHs with O-/B-type companion stars, HD 130298 in the Milky Way (Mahy et al. 2022) and VFTS243 in the Large Magellanic Cloud (Shenar et al. 2022), also differ substantially in their eccentricities: VFTS243 is an almost exactly circular system, while the strong candidate HD 130298 has a high eccentricity $e = 0.47$. A number of additional spectroscopic dormant BH candidates are still debated (Thompson et al. 2019; Jayasinghe et al. 2021; Bodensteiner et al. 2022; Zak et al. 2023; Chakrabarti et al. 2023), and several long-debated candidates were recently found to be BH impostors (e.g., Müller-Horn et al. 2026).

Gaia astrometry holds great promise for the detection of several dozen new dormant systems and candidates with the forthcoming fourth data release (hereafter *Gaia* DR4, Breivik et al. 2017; Wiktorowicz et al. 2020; Chawla et al. 2022, 2025; Shikauchi et al. 2022; Shahaf et al. 2023; El-Badry 2024a; Nagarajan et al. 2025). Currently, we know of three *Gaia* dormant BHs (El-Badry et al. 2023b,a; Tanikawa et al. 2023; Gaia Col-

⋆ e-mail: mapelli@uni-heidelberg.de

Article published by EDP Sciences, to be cited as https://doi.org/10.1051/0004-6361/202660419

laboration et al. 2024). The BH masses of *Gaia* BH1 and BH2 are $\sim$ 9 M$_\odot$, whereas BH3 is the only known electromagnetic stellar origin BH with a mass above 30 M$_\odot$. Interestingly, the metallicity of the companion to BH3 is low ([Fe/H]=–2.64, Gaia Collaboration et al. 2024), corroborating the idea that more massive BHs exist in metal-poor systems because of failed supernovae (Woosley et al. 2002; Mapelli et al. 2009; Belczynski et al. 2010). Moreover, BH3 is associated with the remnant of a disrupted globular cluster (Balbinot et al. 2024), which might indicate a dynamical origin of the system (Marín Pina et al. 2024, 2026), although a primordial binary system is not excluded (El-Badry 2024b; Iorio et al. 2024) because the orbital period is relatively long ($\sim$ 11.6 years).

Gaia BH1 and BH2 are challenges for stellar and binary evolution theory because of their orbital properties. Specifically, their orbital periods are 185 and 1277 days, respectively. In both cases, but especially for *Gaia* BH1, the orbital period is considered to be too long to be explained by a post-common-envelope system and too short to originate from a non-interacting system. If the initial orbital separation was short enough to lead to the onset of a Roche-lobe overflow, we indeed expect that the BH1 and BH2 progenitors underwent an unstable mass-transfer episode, that is, a common-envelope (CE) phase (Paczyński & Ziółkowski 1968; Ge et al. 2015), given the extreme mass ratio at the time of binary formation ($q = m_1/m_2 > 20$). According to the traditional α formalism for CE evolution, the expected final orbital period would be a few days, unless the CE ejection efficiency parameter $\alpha > 10$ (El-Badry et al. 2023b). Moreover, the orbital eccentricities of *Gaia* BH1 and BH2 are high, which is usually disfavored after a CE episode, unless the BH formed with a strong natal kick.

A dynamical formation channel in a stellar cluster (Shikauchi et al. 2020; Rastello et al. 2023; Di Carlo et al. 2024; Tanikawa et al. 2024a; Marín Pina et al. 2024; Fantoccoli et al. 2025) or in a hierarchical triple (Hayashi et al. 2023; Generozov & Perets 2024; Li et al. 2024, 2026a) is free of this problem, but *Gaia* BH1 and BH2 are currently not inside a cluster: they must have evaporated or been ejected from their parent cluster long ago. Interestingly, other types of post-mass-transfer binaries, for example, the systems detected by *Gaia* hosting white dwarfs (Yamaguchi et al. 2025) or neutron stars (El-Badry et al. 2024; Tanikawa et al. 2024b; Chattopadhyay et al. 2026), share the same interpretational challenges. Dynamical formation is a reasonable option for dormant BHs because dynamical exchanges favor the formation of more massive systems (Hills & Fullerton 1980), but is quite unlikely for white dwarf and neutron star binaries.

Alternative explanations include the possibility that massive stellar radii evolve in a more compact way than traditionally expected (Gilkis & Mazeh 2024) or that stellar winds are more effective than currently modeled (Kruckow et al. 2024; Sabhahit et al. 2023; Boco et al. 2025; Pauli et al. 2026; Romagnolo et al. 2026). In binary evolution processes, non-conservative mass transfer can lead to a substantial widening of the orbit, especially when angular momentum is lost as a wind at the surface of the donor star (Vinciguerra et al. 2020). Recently, Olejak et al. (2025) demonstrated through binary evolution models with the code MESA (Paxton et al. 2011, 2018) that this type of non-conservative mass transfer can indeed lead to orbital periods compatible with *Gaia* BH1 and BH2. Non-conservative mass transfer is favored for the progenitors of such systems, considering that the accretor (i.e., the companion of the BH progenitor) is a low-mass star and its Kelvin-Helmholtz timescale therefore is $O(10)$ Myr long.

Here, we perform a large parametric study to explore the formation of the *Gaia* BHs from isolated binary systems with the population-synthesis code SEVN (Spera et al. 2019; Mapelli et al. 2020; Iorio et al. 2023). Our simulations do not depend on the stellar evolution models described by Hurley et al. (2000), but are based on current stellar tracks adopting observationally calibrated core-overshooting parameters and wind mass-loss (Costa et al. 2025). We explore the effect of accretion efficiency, mass-transfer stability, angular momentum transport, and core-collapse supernova (CCSN) prescriptions. For the first time in the context of dormant BHs, we explore the possibility that BH natal kicks are not modulated by fallback.

We find that the orbital eccentricity and period of *Gaia* BH1, BH2, and BH3 favor relatively strong natal kicks, similar to those expected for neutron stars. Models in which the natal kicks are weak, for instance, because they are modulated by fallback, result in the formation of a large population of dormant BHs with long orbital periods ($P_{\rm orb} > 10^4$ days), which will be tested soon by the fourth *Gaia* data release. Our models confirm that the traditional α CE model with a CE ejection efficiency $\alpha < 1$ is a poor description of the evolution of the *Gaia* BHs. In contrast, highly non-conservative stable mass transfer is an alternative way to explain the orbital periods of *Gaia* BH1 and BH2, especially when we assume that angular momentum is lost from the surface of the donor star.

2. Methods

2.1. Population synthesis with SEVN

The stellar evolution for N-body code SEVN evolves stellar properties through on-the-fly interpolation of precomputed stellar tracks (Spera & Mapelli 2017; Spera et al. 2019; Mapelli et al. 2020; Iorio et al. 2023). We used the stellar tracks evolved with PARSEC (Bressan et al. 2012; Costa et al. 2025), including stellar masses down to 0.7 M$_\odot$ (Nguyen et al. 2025). SEVN models binary evolution with semi-analytical prescriptions. We refer to Iorio et al. (2023) for a detailed description of the code. Here, we highlight the main differences between the default SEVN setup presented by Iorio et al. (2023) and our models below.

2.2. Natal kicks

BHs and neutron stars receive a natal kick at birth. We considered two alternative models for the natal kick. Model DM25 assumes that the natal kicks of BHs and neutron stars follow a lognormal distribution with a mean value $\mu = 5.60$ and a standard deviation $\sigma = 0.68$, adopting the fit by Disberg & Mandel (2025, hereafter DM25) to the proper motion of young Galactic pulsars (Hobbs et al. 2005). This distribution peaks at 150–200 km s^{-1}. Model DM25fb starts from the same distribution as DM25, but then corrects the kick values by accounting for the fallback parameter, namely $v_k = (1 - f_{\rm fb})\, v_{\rm DM25}$, where $v_{\rm DM25}$ is a random number derived from the DM25 lognormal distribution, and $f_{\rm fb}$ is the is the fraction (from 0 to 1) of the stellar envelope mass that falls back (Fryer et al. 2012). Previous works always assumed that BH natal kicks are modulated by fallback (Shikauchi et al. 2022; Kruckow et al. 2024; Chawla et al. 2025) or that BHs received no natal kicks (Shikauchi et al. 2022), despite evidence that at least a fraction of Galactic BHs are born with substantial kicks (Fragos et al. 2009; Repetto et al. 2017; Atri et al. 2019; Nagarajan & El-Badry 2025). The properties of our models are summarized in Table A.1.

2.3. Core-collapse supernova (CCSN) model

In our analysis, we used three simplified models to remap the final properties of the star at the onset of core collapse to the mass of the compact remnant. The delayed (D) and rapid (R) models were the same as described by Fryer et al. (2012); they are both fitting formulas to one-dimensional semi-analytic CCSN models and only depend on the total mass bound to the star and the carbon-oxygen core mass at the end of carbon burning. The only difference between the two original models is the assumed timescale to revive the shock, which is short (< 250 ms) in the rapid model and long (> 500 ms) in the delayed model. The compactness (C) model takes the compactness parameter as defined by O'Connor & Ott (2011) $\xi_{2.5} \equiv 2.5\,\mathrm{M}_\odot\,[10^3\,\mathrm{km}/R(2.5\,\mathrm{M}_\odot)]$ into account, where $R(2.5\,\mathrm{M}_\odot)$ is the radius that encloses a mass of 2.5 $\mathrm{M}_\odot$. We calculated the compactness at the onset of core collapse by using the fitting formula derived by Mapelli et al. (2020). We assumed that stellar models with $\xi_{2.5} \geq 0.3$ ($\xi_{2.5} <$ 0.3) form BHs (neutron stars). In all the considered CCSN models, we corrected the final mass of the compact remnant to account for neutrino mass loss, as described by Zevin et al. (2020).

2.4. Mass transfer and angular momentum transport

We modeled wind mass transfer and Roche-lobe overflow mass transfer as described in Iorio et al. (2023) and largely based on Hurley et al. (2002). Specifically, in Roche-lobe overflow, the mass-accretion rate of a non-degenerate accretor is equal to $\dot{M} = f_\mathrm{a}\,|\dot{M}_\mathrm{d}|$, where $\dot{M}_\mathrm{d}$ is the rate of mass lost by the donor, and $f_\mathrm{a} \in [0, 1]$ is a constant efficiency parameter. For degenerate accretors (compact objects), the mass-accretion rate is limited by the Eddington value. Because the accretor is a solar-mass star in our case, the Kelvin-Helmholtz timescale is quite long ($\sim$ 10 Myr), and thus, we expect f_a to be rather small.

If $f_\mathrm{a} < 1$, accretion is non-conservative, and angular momentum is lost. We considered two options for angular momentum loss: isotropic re-emission, and Jeans mode. In the isotropic re-emission model (Isot), angular momentum is lost as an isotropic wind from the accretion disk. Hence, the loss of orbital angular momentum scales as $\Delta J \propto \Delta M\,M_\mathrm{d}/(M_\mathrm{a} + M_\mathrm{d})$, where ΔM is the mass lost, M_d is the donor mass, and M_a is the accretor mass. In the Jeans mode, angular momentum is lost as an isotropic wind from the donor star, and $\Delta J \propto \Delta M\,M_\mathrm{a}/(M_\mathrm{a} + M_\mathrm{d})$. In our case, since $M_\mathrm{a} \ll M_\mathrm{d}$, the Isot mode results in a much larger angular momentum loss than the Jeans mode, thus leading to a more efficient orbital shrinking than the latter. Since the donor star is an O-type star with very fast winds ($\sim$ 1000 km s^{-1}), the Jeans mode might be physically closer to the description of a *Gaia* BH-like progenitor (Olejak et al. 2025).

2.5. Common-envelope (CE) evolution

In SEVN and other population-synthesis codes, mass transfer is assumed to become unstable when the donor-to-accretor mass ratio is above a given threshold q_c, whose value depends on the properties of the donor. We assumed the same values of q_c as in the original paper by Hurley et al. (2002). The q_c values are listed in Appendix B. When mass transfer was unstable, we used the α formalism in the version detailed by Hurley et al. (2002) to describe the orbital evolution of the system and the chance of ejecting the envelope. Here, α is an efficiency parameter, describing which fraction of the orbital energy released during the inspiral of the cores is converted into energy available to unbind the envelope. In our models, we considered values of α = 0.1, 0.5, 1 (fiducial model), 2, 3, 5, 7, 10, and 15. Values of $\alpha > 1$ are unphysical according to the original definition of this parameter. They are usually included in population-synthesis simulations with the idea of taking additional sources of energy into account (e.g., recombination, nuclear reactions, or outflows) that are not included in the traditional $\alpha-$formalism (e.g., Zorotovic et al. 2011; Ivanova et al. 2013; Giacobbo & Mapelli 2018; Fragos et al. 2019; El-Badry et al. 2023a; Li et al. 2026b).

The α formalism is a simplistic approximation to describe CE evolution (e.g., Ivanova et al. 2013; Röpke & De Marco 2023). For this reason, we also considered models in which we set q_c to an unphysically high value (q_c = 2000) to prevent the system from starting a CE evolution. With this, we do not claim that the progenitor of the *Gaia* BHs did not undergo unstable mass transfer. We instead wished to quantify the differences in the evolution of such systems when we consider two different models of orbital evolution during mass transfer (we refer to Olejak et al. (2025) for an accurate discussion of these two scenarios). In general, using the α formalism with $\alpha \leq 1$ produces an efficient shrinking of the semi-major axis, also by several orders of magnitude. Even when we set q_c = 2000, SEVN triggered unstable mass transfer when both stars in the binary filled their Roche lobes or when a collision took place (i.e., when the pericenter distance between two stars becomes smaller than the sum of their radii).

2.6. Initial conditions

We sampled the masses of the primary star (M_1) from a Kroupa initial mass function (Kroupa 2001) $\mathcal{F}(M_1) \propto M_1^{-2.3}$ in a range between 15 and 150 $\mathrm{M}_\odot$. We did not simulate lower-mass primary stars because we were only interested in BH progenitors.

We drew the secondary star mass (M_2) within the range $[0.7, 150]\,\mathrm{M}_\odot$ from the distribution $\mathcal{F}(q) \propto q^{-0.1}$, where $q = M_2/M_1$ (Sana et al. 2012) and $0.01 \leq q \leq 1$.

The orbital periods and eccentricities were also drawn from the distributions derived by Sana et al. (2012) by fitting the properties of a sample of O-type binary stars in open clusters. Specifically, we randomly sampled the orbital periods P_orb and the eccentricities e from the distributions $\mathcal{F}(P_\mathrm{orb}) \propto (\log P_\mathrm{orb})^{-0.55}$, with $0.15 \leq \log(P_\mathrm{orb}/\mathrm{d}) \leq 5.5$, and $\mathcal{F}(e) \propto e^{-0.42}$, with $0 \leq e \leq 1 - (P/2\,\mathrm{days})^{-2/3}$, following the correction by Moe & Di Stefano (2017). In Appendix C we consider a set of runs starting with a thermal distribution for the initial eccentricities $\mathcal{F}(e) \propto e$ for comparison with Shikauchi et al. (2022).

We sampled 10^7 binaries and used them as initial conditions for each considered run. We considered three different metallicities: Z = 0.014, 0.017, and 1.4×10^{-4}. The properties of our models are summarized in Table A.1.

3. Results

3.1. Effect of natal kicks

Figures 1 and 2 show the behavior of orbital period, eccentricity, BH mass (M_BH), and companion mass (M_*) of the simulated systems in models Afb and A, respectively. The only difference between the two models is the formalism for natal kicks. In model A, we drew the natal kicks from the distribution by DM25, whereas in model Afb, the kicks were reduced taking the fallback into account, as described by Fryer et al. (2012).

The difference is striking: when the kicks are suppressed by fallback (Fig. 1), we expect a large population of systems with almost zero eccentricity and long orbital periods ($P > 10^3$ days), while the orbital period and eccentricity of a small fraction ($\sim 0.01 - 0.02$) of the simulated dormant systems lie in the range of *Gaia* BH1 and BH2.

Instead, when the kicks are drawn from the distribution by DM25, most of the systems with a long orbital period are disrupted by the natal kick. The orbital period and eccentricity of a higher fraction of the simulated systems ($\sim 0.1 - 0.3$) lie in the range of *Gaia* BH1 and BH2.

Moreover, the overall number of dormant BH systems predicted by model A is lower by a factor of ≈ 60 (Table A.1) than that predicted by model Afb, because stronger natal kicks (model A) disrupt the systems with initially long orbital periods.

This consideration applies to all the other models we simulated (Appendices A, B, and C): when the natal kicks were modulated by fallback, the dormant BH population we recovered was extremely numerous and dominated by systems with long ($P > 10^3$ days) orbital periods. Such long-period systems mostly host massive BHs (> 12 M$_\odot$) because these form via failed supernovae and are assumed to have weak or no natal kicks in the fallback formalism. *Gaia* DR4 will probe the existence of this class of long-period massive BH systems (Nagarajan et al. 2025), yielding constraints on the natal kicks of BHs.

Qualitatively, models in which the BH natal kick does not depend on fallback and is similar to the distribution inferred for the Galactic young pulsars (DM25) are able to produce systems with the orbital properties of *Gaia* BH1 and BH2.

Appendix C shows that the main takeaway of this section does not change when we assume high initial orbital eccentricities: natal kicks modulated by fallback result in the formation of a population of non-interacting long-orbital-period ($P > 10^3$ days) systems, which is instead completely suppressed when natal kicks are stronger. However, the final eccentricities of the long-orbital-period systems formed in the fallback models strongly depend on the initial eccentricity distribution: high (low) initial eccentricities lead to high (low) final eccentricities of the BH systems with long orbital periods, because these do not undergo Roche-lobe overflow during their life.

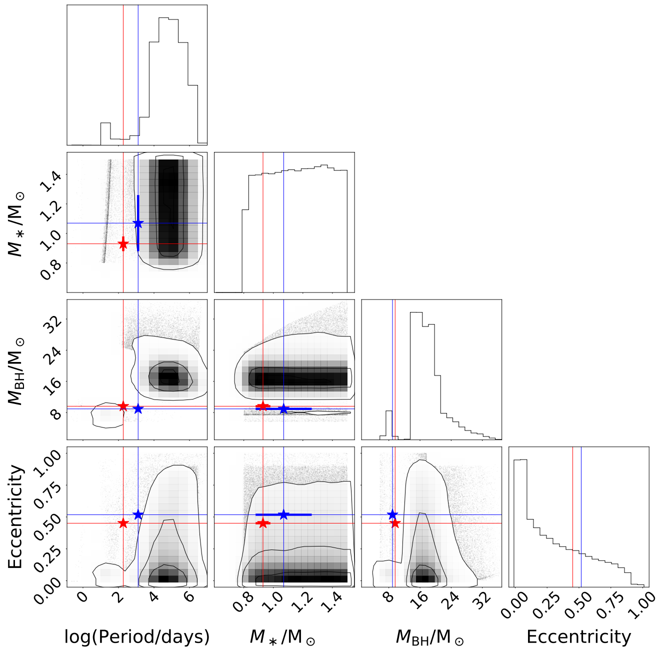

Fig. 1. Corner plot showing the orbital period, eccentricity, BH mass ($M_{\rm BH}$), and companion star mass (M_*) in the simulations of model Afb. In this model, natal kicks are drawn from DM25 and modulated by fallback, the rapid CCSN model is assumed (Fryer et al. 2012), the accretion efficiency is $f_{\rm a} = 0.5$, angular momentum transport follows the isotropic re-emission assumption, the critical mass ratios for mass-transfer instability are taken from Hurley et al. (2002), CE evolution assumes $\alpha = 1$, and the metallicity is approximately solar ($Z = 0.014$). The contour levels of this and the other corner plots show the 20%, 50%, and 90% probability regions. The red and blue stars show the values for *Gaia* BH1 (El-Badry et al. 2023b) and BH2 El-Badry et al. (2023a) and their corresponding 1σ uncertainties (smaller than the markers in most cases).

3.2. Stable mass transfer

When Roche-lobe overflow starts in a system like the progenitor of *Gaia* BH1 and BH2, with a mass ratio $q \gtrsim 20$ between donor (i.e., the BH progenitor) and accretor, it is thought to lead to unstable mass transfer given the long Kelvin-Helmholtz timescale of the accretor (~ 10 Myr for a Sun-like star). The description of unstable mass transfer in population-synthesis codes is mostly implemented through the α formalism for CE evolution (Hurley et al. 2002). For many years, we have been aware that the α formalism for CE evolution is an overly simplified model (Ivanova et al. 2013; Röpke & De Marco 2023), but we generally use it as a parametric toy model in population synthesis because of its simplicity. In this section, we simply make an experiment and assume that the mass transfer of the possible progenitor systems was always stable. We use this assumption only as a thought experiment, but we refer to the work by Olejak et al. (2025) and Ge et al. (2020) for a discussion of the stability of similar systems. Here, we set up SEVN so that the mass-ratio threshold for mass transfer to become unstable was never reached (critical mass ratio $q_c = 2000$).

Figure 3 shows model BJ, where we assumed that mass transfer is stable, the accretion efficiency is zero ($f_{\rm a} = 0$), and angular momentum is lost from the system as a wind from the donor star (the so-called Jeans mode). The natal kicks were drawn from DM25. For comparison, Fig. 4 shows model B,

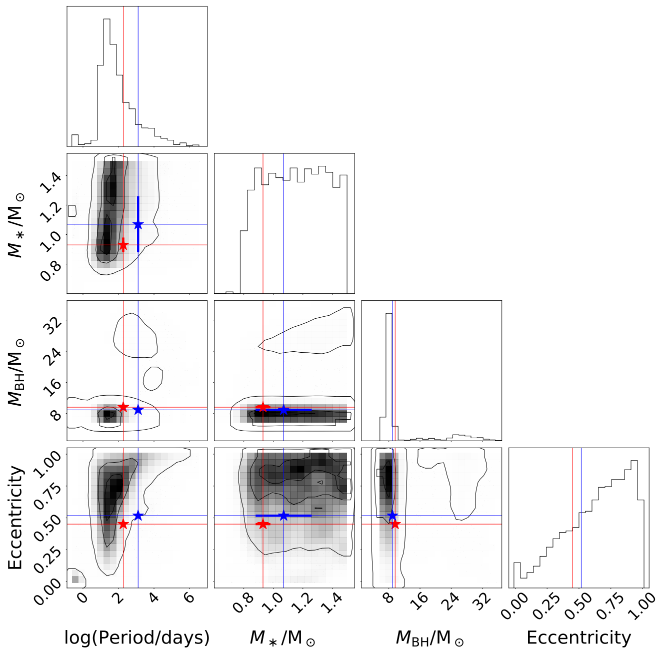

Fig. 2. Same as Fig. 1, but for model A. The only difference between the two models is that model A assumes natal kicks from DM25 whereas model Afb takes into account the fallback to estimate natal kicks.

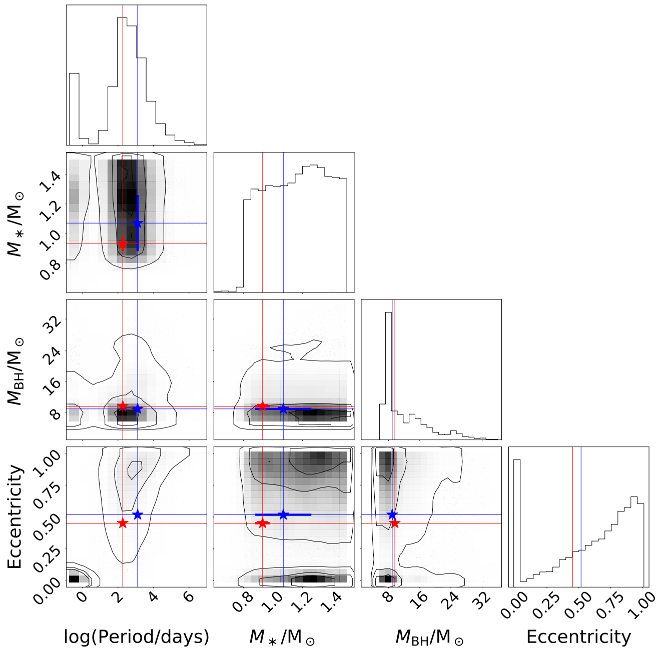

Fig. 3. Same as Fig. 1, but for model BJ, in which we prevented the onset of CE evolution by setting a critical mass ratio $q_c = 2000$. In this model, natal kicks are drawn from DM25 (no fallback), the rapid CCSN model is assumed (Fryer et al. 2012), the accretion efficiency is $f_a = 0.0$, angular momentum transport follows the Jeans mode, and the metallicity is approximately solar ($Z = 0.014$).

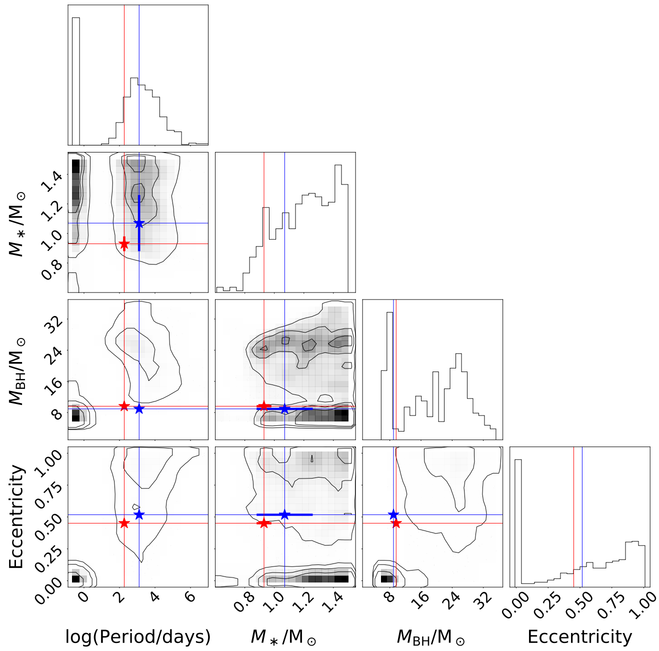

Fig. 4. Same as Fig. 3, but for model B. This model is the same as model BJ (i.e., mass transfer is always assumed to be stable), but for two differences: the accretion efficiency is $f_a = 0.5$ (instead of $f_a = 0.0$ as in model BJ), and angular momentum transport follows the isotropic re-emission (instead of Jeans mode as in model BJ).

which differs from BJ only in that the accretion efficiency is $f_a = 0.5$ and angular momentum is lost according to the isotropic re-emission formalism.

Requesting that mass transfer is always stable instead of allowing for CE evolution helps us to produce systems with the period of *Gaia* BH1 and BH2 especially (but not only) with kicks from DM25. However, many more systems merge or circularize when we assume a high accretion efficiency ($f_a \geq 0.5$) and isotropic re-emission compared to low accretion efficiency and Jeans mode. For instance, model B shown in Fig. 4 (with $f_a = 0.5$ and isotropic re-emission) produces fewer BH systems by a factor of ≈ 7 than model BJ (Fig. 3). About 25% and 14% of the systems shown in Fig. 4 and Fig. 3 have circularized at the end of the simulation, respectively. The reason for these differences is that a dissipative mass transfer with the Jeans mode keeps the orbital period longer than a more conservative mass transfer with isotropic re-emission (Olejak et al. 2025). Hence, many more binaries merge in the isotropic re-emission case, whereas the survivors tend to circularize during mass transfer.

Models that assume no CE evolution, accretion efficiency $f_a \sim 0$, and the Jeans mode for angular momentum transport maximize the probability of forming systems like *Gaia* BH1 and BH2, according to our metrics (Tab. A.1).

3.3. Black hole mass function

To determine the mass of the BH from the properties of the progenitor at the onset of core collapse, SEVN uses several formalisms obtained from 1D CCSN models. Figures 2 and 3 adopt the rapid model by Fryer et al. (2012). Figures 5 and 6 are the same as Fig. 2, but for other CCSN models, based on the compactness parameter (O'Connor & Ott 2011) in Fig. 5 (see model C) and the delayed model (Fryer et al. 2012) in Fig. 6. The comparison of these figures shows that with the rapid model, we expect a peak in the BH mass range at $\approx 8 - 10$ M$_\odot$, similar to the mass of *Gaia* BH1 and *Gaia* BH2. In contrast, delayed and compactness models tend to produce many lower-mass systems.

However, with weak kicks (based on the fallback criterion), all the CCSN models predict a large population of massive ($\sim 16 - 32$ M$_\odot$) BHs in binary systems with low-mass stars. *Gaia* DR4 will definitely probe the existence of this subpopulation (Nagarajan et al. 2025).

3.4. CE efficiency parameter

Increasing the CE efficiency parameter α from 0.1 to 15 leads to dormant BHs with progressively longer orbital period and higher eccentricities, especially when only strong natal kicks are considered (according to the DM25 distribution without modulation by fallback). This happens because higher values of α correspond to a more efficient ejection of the envelope with less orbital shrinking. As a result, models with $\alpha < 1$ cannot reproduce the orbital properties of the observed *Gaia* BHs, because they predict systems with orbital periods that are too short. In contrast, models with $\alpha \geq 1$ produce similar results (in terms of orbital period and eccentricity distribution) as our stable mass-transfer models with low accretion efficiency ($f_a \sim 0$) and Jeans mode for angular momentum loss.

Our result agrees with those of previous works in finding a preference for $\alpha \geq 1$ (Giacobbo & Mapelli 2018; Mapelli & Giacobbo 2018; Fragos et al. 2019; Hirai & Mandel 2022; El-Badry et al. 2023a). This might support the importance of additional sources of energy for unbinding the CE, or the need for a different formalism to describe orbital evolution during a CE phase (Nelemans et al. 2000; Nelemans & Tout 2005; Fragos et al.

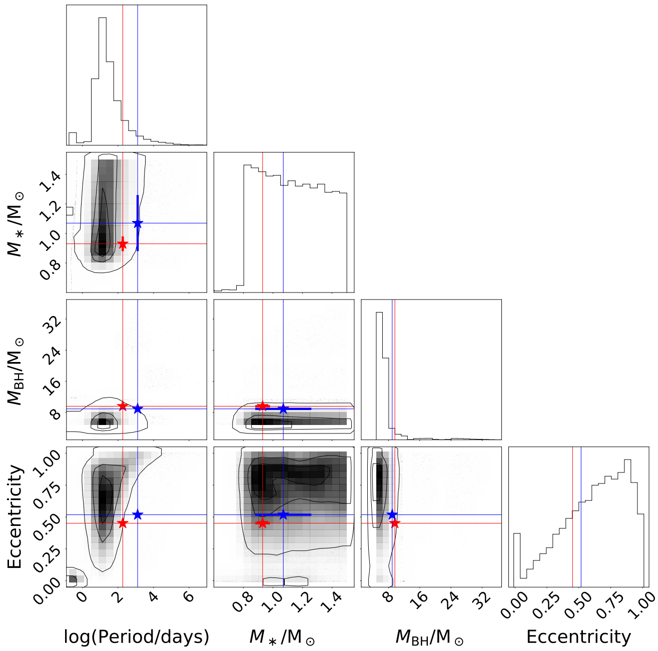

Fig. 5. Same as Fig. 2, but for model C. This model is the same as model A, but for one difference: it assumes the compactness criterion by O'Connor & Ott (2011) for the outcome of a CCSN.

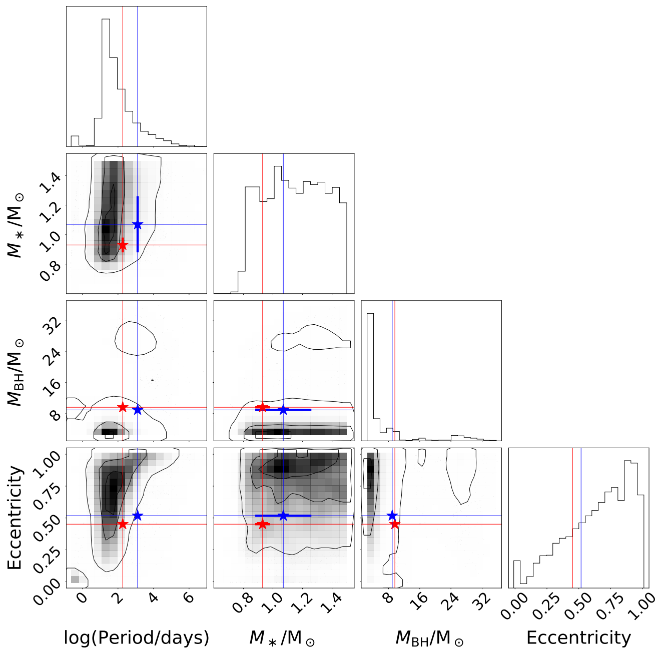

Fig. 6. Same as Fig. 2, but for model D. This model is the same as model A, but for one difference: it assumes the delayed formalism by Fryer et al. (2012) for the outcome of a CCSN.

2019; Hirai & Mandel 2022). We further discuss the models with $\alpha \neq 1$ in Appendix B.

3.5. Metallicity and *Gaia* BH3

Gaia BH3, an anticipation of *Gaia* DR4, is substantially different from BH1 and BH2. The metallicity of the companion is well below solar ([Fe/H] = −2.64), the mass of the BH is ≈ 33

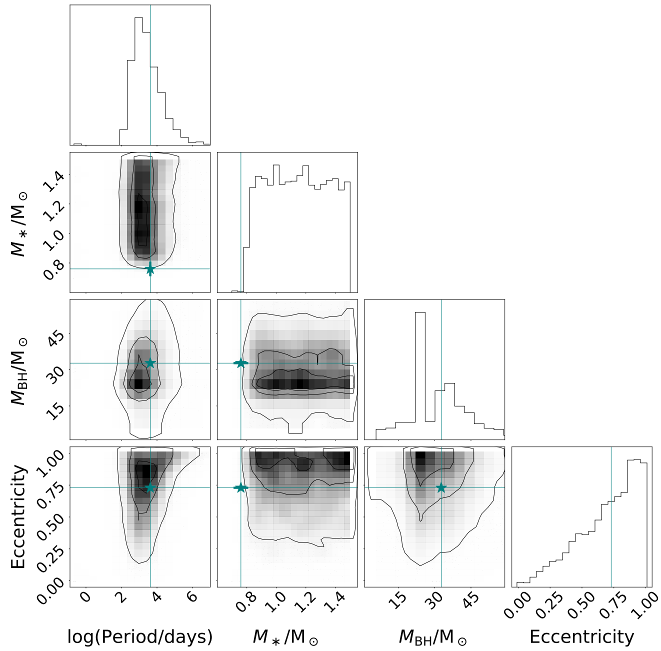

Fig. 7. Same as Fig. 1, but for model AJlowZ. This model is the same as AJ (with CE $\alpha = 1$, accretion efficiency $f_a = 0$, Jeans mode for angular-momentum loss, and natal kicks from DM25), but with metallicity $Z = 1.4 \times 10^{-4}$. Only *Gaia* BH3 is shown for comparison (green lines and stars).

$M_\odot$, and the orbital period is around 4000 days (Gaia Collaboration et al. 2024). The orbital eccentricity is also high ($e \approx 0.75$). Figure 7 shows model AJlowZ. This model has a low metallicity $Z = 1.4 \times 10^{-4}$. Similar to BH1 and BH2, also BH3 is more likely formed with a low accretion efficiency and the Jeans mode for angular momentum transport, but unlike the other two *Gaia* BHs, a CE evolution is the configuration that maximizes the probability of producing a *Gaia* BH3-like system (Table A.1).

Overall, this result clearly shows the relatively minor difference between our best CE and non-CE evolution systems: the most important ingredients to form *Gaia* BH1, BH2, and BH3 seem to be the strong natal kicks (DM25), the low accretion efficiency ($f_a = 0$), and the Jeans mode for angular momentum transport. The latter keeps the binary orbital period relatively wide, while the kick is essential to produce high eccentricities.

4. Discussion

4.1. Evolutionary channels

Our simulations demonstrated that two main evolutionary channels are able to produce *Gaia* BH-like systems from isolated binaries: stable mass transfer, and CE evolution. Figures 8 and 9 display the temporal evolution of some specific simulations from models BJ and Afb as examples of stable mass transfer and CE evolution, respectively. The two figures show the systems with the final masses, orbital periods, and eccentricities closest to the measured values of *Gaia* BH1.

In the first channel (Fig. 8; the stable mass-transfer channel), the zero-age main-sequence mass of the primary star spans from ≈ 30 to ≈ 90 $M_\odot$, and the initial orbital period P_{in} is shorter than the final period ($P_{in} \approx 10-50$ days). This channel only becomes important when mass transfer remains stable, is highly dissipative ($f_a \sim 0$), and when mass/angular momen-

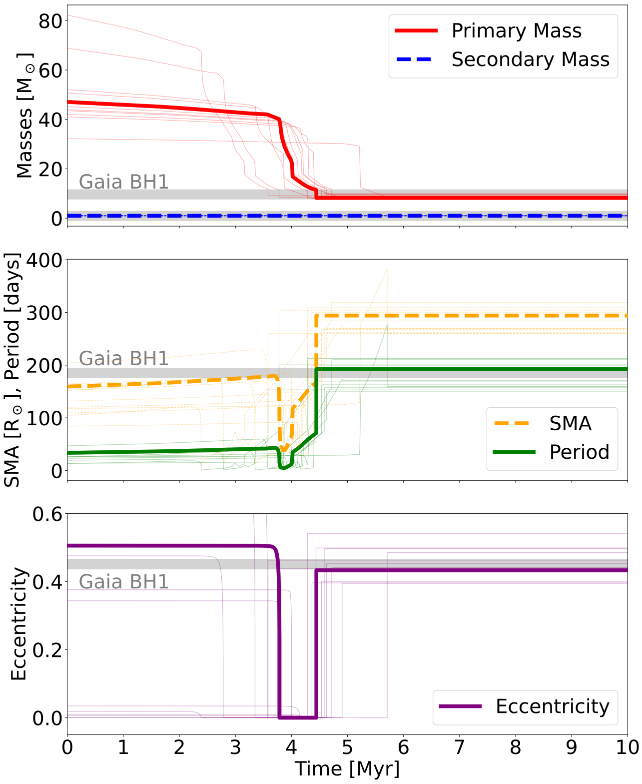

Fig. 8. Evolution of the best-matching *Gaia* BH1-like systems through stable mass transfer. We show model BJ (same model as Fig. 3), with stable mass transfer (q_c = 2000), f_a = 0, Jeans mode, and no fallback. From top to bottom: Temporal evolution of the primary and secondary mass, semi-major axis (SMA), orbital period, and eccentricity. The thick line shows the best-matching model among all the simulated systems, and the thin lines show the next best-matching models.

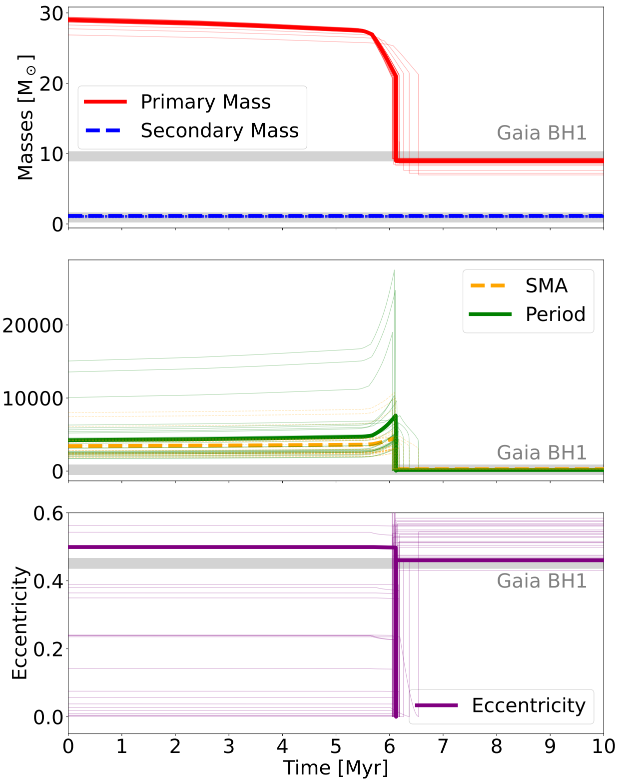

Fig. 9. Same as Fig. 8, but considering the best-matching *Gaia* BH1-like systems formed through CE evolution. We show model Afb (same model as Fig. 1), with CE evolution, α = 1, f_a = 0.5, isotropic re-emission, and fallback.

tum are lost as a wind from the donor (Jeans mode). In this case, the orbit shrinks by a factor of $\lesssim 2$ during mass transfer. The CCSN happens during stable mass transfer, and the natal kick sets the final period and eccentricity. Without a significant kick ($v_{\rm kick} \approx 30 - 100$ km/s), it is not possible to attain the observed eccentricity of the *Gaia* BHs, because we assumed that the orbit circularizes during Roche-lobe overflow (see, e.g., Kotko et al. 2024).

The second formation channel (Fig. 9; the CE-evolution channel) produces all the *Gaia* BH-like systems in the runs where CE evolution is activated. In this case, when α = 1, the initial mass of the primary star is 25–30 M$_\odot$ (the range is very narrow because the final semi-major axis depends on the donor mass in the traditional α formalism), the initial semi-major axis is higher by at least a factor of 10 than the final semi-major axis, and the orbit shrinks dramatically during the CE phase. As in the other formation channel, the natal kick is crucial for determining the final eccentricity of the system.

4.2. Percentile distribution

To quantitatively assess whether the models we presented are capable of producing BHs with parameters similar to *Gaia* BH1, BH2, and (for $Z = 1.4\times10^{-4} \approx 10^{-2}$ Z$_\odot$) BH3, we considered the percentiles of the model probability distribution function (PDF) at which the *Gaia* BHs are found. This approach allowed us to quickly identify models for which the observations are no plausible outcome. The main caveat is that this analysis did not include selection effects.

In practice, we approximated the PDF of each model with a Gaussian-mixture model, trained on the samples produced by the population-synthesis code with FIGARO (Rinaldi & Del Pozzo 2024), and we evaluated the approximated PDF for each of the available samples. When these samples were ranked according to their PDF, we used them as an approximate one-dimensional percentile grid. To account for the measurement uncertainty of the *Gaia* BHs, we used a Monte Carlo approach and drew 100 samples for each object from a multivariate Gaussian distribution centered on the measured values and with a standard deviation equal to the measurement uncertainty. We neglected possible correlations between parameters. For each of these samples, we evaluated the PDF and computed the corresponding percentile.

Table A.1 reports the median percentile value and the 68% credible interval for each model and object. The percentiles for the majority of the models are higher than 95. The models highlighted in blue recover the properties of at least one of the *Gaia* BHs within the ≤ 90th percentile.

4.3. Selection effects

The percentile-based approach described above quantifies the probability of forming *Gaia* BHs with the observed properties for a given model. However, it does not account for observational selection effects. In particular, systems that are intrinsically rare can still be preferentially detected, while models that efficiently produce *Gaia* BH-like systems can over- or underpredict the total number of detectable sources.

We provide an order-of-magnitude estimate of the number of dormant BHs that would have been detected in the third *Gaia* data release (*Gaia* DR3) for our different models. To do this, we adopted a forward-modeling approach. First, we scaled our simulated populations to the Milky Way to estimate the total number of *Gaia* BH systems. Second, we generated mock observations of these binaries to emulate *Gaia* measurements. Finally, we applied a model of the *Gaia* non-single star selection function to estimate the number of systems that would have been detected as binaries in DR3.

Here, we focus on models Afb (Fig. 1) and A (Fig. 2) as examples of runs in which natal kicks are modulated and are not modulated by fallback, respectively. In our models Afb and A, the number of dormant BHs with a main-sequence or a giant companion in the mass range $0.7-1.5\,\mathrm{M}_\odot$ is N_dorm =108347 and 1932, respectively. For BH masses in the range 8–12 $\mathrm{M}_\odot$, these numbers are reduced to 2161 and 576, respectively.

The total initial mass of our stellar population is $M_\mathrm{sim} = 2.32\times10^9\,\mathrm{M}_\odot$ (after correcting for the low-mass stars that we did not simulate), corresponding to approximately 5% of the stellar mass in the Milky Way (Licquia & Newman 2015; Bland-Hawthorn & Gerhard 2016). However, we assumed that all stars are initially members of binary systems, leading to an overestimate by a factor of $\gtrsim 2$ of the binary star population. The actual correction factor depends on the mass of the primary star, but here we only consider an order-of-magnitude estimate (Moe & Di Stefano 2017). In addition, at solar metallicity, the stellar evolution reduces the total mass of a stellar population older than ~ 1 Gyr to $\sim 50\%$ of its initial value due to winds and supernovae, implying a correction factor $f_\mathrm{loss} \sim 0.5$. We neglected variations in metallicity across the Milky Way for this estimate.

Combining these factors, we estimate the total number of dormant BH systems in the Milky Way for the model A as

$$N_\mathrm{dorm,MW} = 4.16\times10^4 \left(\frac{N_\mathrm{dorm}}{1932}\right)\left(\frac{M_\mathrm{MW}}{5\times10^{10}\,\mathrm{M}_\odot}\right) \left(\frac{2.32\times10^9\,\mathrm{M}_\odot}{M_\mathrm{sim}}\right)\left(\frac{f_\mathrm{bin}}{0.5}\right)\left(\frac{0.5}{f_\mathrm{loss}}\right), \quad (1)$$

where M_MW is the current total stellar mass of the Milky Way, and $f_\mathrm{bin} = 0.5$ is the fraction of stars in binary systems.

The number of detected *Gaia* BHs is related to the total population by the detection probability p_det. We estimate p_det by generating mock observations of the simulated BH binaries, forward-modeling the selection effects of *Gaia*, and counting the fraction of systems that would be detectable. We describe this procedure in Appendix D. We estimate $p_\mathrm{det} = 2.9\times10^{-4}$ and 8.0×10^{-5} for models A and Afb. Combining this with our estimate of the total number of dormant BHs in the Milky Way, we obtain an order-of-magnitude prediction for the number of *Gaia* BHs detectable in DR3,

$$N_\mathrm{det} = 12\left(\frac{p_\mathrm{det}}{0.00029}\right)\left(\frac{N_\mathrm{dorm,MW}}{41600}\right), \quad (2)$$

for model A. This number rises to 186 for model Afb.

This estimate exceeds the effectively detected number of *Gaia* BHs by approximately one (two) order(s) of magnitude for model A (model Afb). We will present a more detailed treatment of selection effects and detectability, including predictions for future *Gaia* data releases, in a follow-up study (Müller-Horn et al., in prep.).

4.4. Formation efficiency

Natal kicks strongly affect the number of dormant BH systems (N_dorm) per total initial stellar mass ($M_\mathrm{sim} = 2.32\times10^9\,\mathrm{M}_\odot$), that is, the efficiency parameter,

$$\eta_\mathrm{dorm} = \frac{N_\mathrm{dorm}}{M_\mathrm{sim}}. \quad (3)$$

As shown in Table A.1, models with fallback yield an efficiency parameter η_dorm of a few $\times10^{-5}\,\mathrm{M}_\odot^{-1}$, which is 20–70 times higher than models run with the DM25 distribution of natal kicks ($\eta_\mathrm{dorm} \sim 10^{-7} - 10^{-6}\,\mathrm{M}_\odot^{-1}$).

The large difference of η_dorm is almost entirely due to the subpopulation of massive dormant BHs ($M_\mathrm{BH} > 12\,\mathrm{M}_\odot$) with a long orbital period ($P_\mathrm{orb} > 10^4$ days) that form when natal kicks are modulated by fallback and are hence strongly quenched for high BH masses. Strong natal kicks ($\gtrsim 100$ km/s) unbind most systems with long orbital periods.

These long-period systems ($> 10^4$ days) are almost undetectable with *Gaia* DR3, but will be accessible to *Gaia* DR4 (Nagarajan et al. 2025). Hence, *Gaia* DR4 will test this scenario and possibly provide indirect constraints on BH natal kicks.

Current observations of dormant systems (Nagarajan & El-Badry 2025) and BHs in X-ray binaries (Fragos et al. 2009; Repetto et al. 2017; Atri et al. 2019) indicate that a significant fraction of BHs in the Milky Way received non-negligible (≈ 100 km s^{-1}) natal kicks, but at least two systems (V404 Cyg and VFTS 243) have a strong preference for weak ($\lesssim 10$ km s^{-1}) natal kicks (Willcox et al. 2025; Nagarajan & El-Badry 2025).

4.5. Comparison with previous work

In this Section, we compare our approach and results to previous work on *Gaia* BHs. In the literature, only Olejak et al. (2025) have explored the Jeans mode with highly non-conservative mass transfer as a possible scenario for the formation of *Gaia* BHs. Similarly to our work, they concluded that stable mass transfer with a low accretion efficiency and Jeans angular momentum transport favors the formation of *Gaia* BH1-like systems. They simulated one specific case with the code MESA (Paxton et al. 2011, 2018), starting with zero initial eccentricity, and did not model BH formation and natal kicks. They suggested that a population-synthesis study exploring mass transfer stability, angular momentum transport, and accretion efficiency is needed to draw statistically significant conclusions about the formation channels of *Gaia* BHs.

Here, we perform such a parameter-space exploration with our code SEVN, which adopts stellar tracks completely different from BSE and other codes based on the fitting formulas derived by Hurley et al. (2000). Specifically, the evolutionary models adopted here come from the PARSEC stellar tracks (Iorio et al. 2023; Nguyen et al. 2025; Costa et al. 2025). We refer to the original papers for details, but mention that these tracks include an accurate modeling of stars close to or above a zero-age main-sequence mass of 100 $\mathrm{M}_\odot$, a large overshooting parameter ($\Lambda_\mathrm{ov} = 0.5$), resulting in larger massive star cores than BSE models, and a radiation-driven wind model including the dependence of mass loss on the Eddington ratio $\Gamma = L/L_\mathrm{Edd}$ (where L and L_Edd are the luminosity and Eddington luminosity, respectively). The inclusion of the mass-loss dependence on the Eddington ratio allowed us to model stellar winds in the optically thick regime (if a star is radiation-pressure dominated) and helps massive stars to avoid the Humphreys-Davidson limit (Gräfener & Hamann 2008; Chen et al. 2015). These features result in a different evolution of the stellar radius compared to BSE (e.g., Fig. 7 of Iorio et al. 2023) and lead to a remarkably different BH mass function even when the same core-collapse supernova model is applied (see Iorio et al. 2023, for a detailed discussion and comparison). Previous work relied on the fitting formulas by Hurley et al. (2000). For example, Shikauchi et al. (2022) used their custom version of BSE with wind models derived from Belczynski et al. (2010), whereas Chawla et al. (2025) used COSMIC, which is also based on BSE for the stellar and binary evolution.

Here, we consider two models for BH natal kicks to compare a scenario in which natal kicks are the same as those of Galactic pulsars (DM25) with one in which they are modulated by fallback (DM25fb). Previous works (e.g., Shikauchi et al. 2022, 2023; Chawla et al. 2022, 2025) assumed zero natal kicks or fallback-modulated kicks for BHs, and they hence resulted in the prediction of a large number of long-period *Gaia* BH-like systems (see, e.g., Fig. 1 of Chawla et al. 2022). In contrast, we also explore cases with BH kicks drawn from the same distribution as neutron star kicks. The possibility that BHs receive significant kicks at birth is compatible with observations (Fragos et al. 2009; Repetto et al. 2017; Atri et al. 2019; Nagarajan & El-Badry 2025), and it significantly helps us to reconcile the estimated merger-rate density of binary BHs with the constraints inferred from gravitational-wave data (e.g., Boesky et al. 2024; Sgalletta et al. 2025).

The models presented in the main text assume low initial orbital eccentricity, following the observational constraints by Sana et al. (2012). In contrast, Shikauchi et al. (2022) drew the initial orbital eccentricities from a thermal distribution, which is usually adopted for the dynamical scenario in star clusters. In Appendix C we show that starting from a thermal eccentricity distribution has almost no effect on the models with DM25 natal kicks but significantly affects the final eccentricity of the long-orbital period systems in the fallback models. Because the long-orbital period systems ($P_{\rm orb} > 10^3$ days) evolve without Roche-lobe overflow, their final eccentricity largely reflects their initial eccentricity if natal kicks are negligible.

For the treatment of stable and unstable mass transfer, previous population-synthesis works assumed the default model of BSE, which relies on the isotropic re-emission formalism for angular momentum transport and on a mostly conservative mass transfer formalism (Hurley et al. 2002). Our results show that the assumption on mass-accretion efficiency and angular momentum transport drastically affect the results. CE evolution has already been thoroughly investigated in previous work with the α formalism, exploring values of the free parameter α from 0.1 to 15 (e.g., Shikauchi et al. 2022; El-Badry et al. 2023b). Here, we show that disabling CE evolution has a major effect on the formation of dormant systems, especially with long orbital periods. We also demonstrate, however, that a non-conservative Jeans mode yields results similar to those of CE evolution with $\alpha \geq 1$.

4.6. Dynamical formation

We did not consider the dynamical channel for dormant BH formation (Rastello et al. 2023; Di Carlo et al. 2024; Marín Pina et al. 2024; Nagarajan et al. 2025), which we will consider in a follow-up study (Marín Pina et al., in prep.). A non-negligible fraction of massive stars form in clustered environments (Lada & Lada 2003), and we already know that *Gaia* BH3 formed in a globular cluster (Balbinot et al. 2024). Rastello et al. (2023) showed that other *Gaia* BHs might have formed in a star cluster as well and were then subsequently ejected from it due to dynamical interactions or cluster evaporation.

Star-cluster dynamics clearly extends the parameter space and introduces more degrees of freedom because the orbital period and eccentricity are affected by dynamical encounters in addition to binary evolution and natal kicks. Star-cluster dynamics can also affect the masses through dynamical exchanges. Interestingly, despite the large parameter space we explored, our models struggle to match the properties of *Gaia* BH3, which is the only *Gaia* BH clearly associated with a globular cluster origin.

Nagarajan et al. (2025) discussed a set of dynamical simulations in which the orbital period of dynamical systems only extended to a few $\times 10^3$ days. In contrast, Rastello et al. (2023), Marín Pina et al. (2024), and Marín Pina et al. (2026) showed dynamical simulations in which the orbital periods of *Gaia* BH-like systems extended to 10^7 days or more. There are several possible explanations for this reason. First, Nagarajan et al. (2025) used the dynamical simulations by Di Carlo et al. (2020), which comprise only 6000 star cluster models, whereas Rastello et al. (2023) analyzed a sample of $> 10^5$ star cluster models. Hence, there might be an effect of low statistics. Moreover, dynamical interactions tend to unbind soft binaries, that is, binary systems with a binding energy lower than the average kinetic energy of a star in the cluster (Heggie 1975). Hence, the maximum orbital period of binary systems in a star cluster depends on the actual threshold between hard and soft binaries, which in turn depends on the velocity dispersion of stars in the cluster.

Based on these considerations, we conclude that adding dynamics to our models is not expected to change the main result of Sect. 3.1: a large population of dormant BHs with orbital periods of $> 10^4$ days would strongly favor models in which BHs are born with weak natal kicks, possibly modulated by fallback. Otherwise, either natal kicks are relatively strong for dormant BHs, or most dormant BHs form in massive ($\gg 10^3$ M$_\odot$) dense clusters, where dormant BH binaries with $P_{\rm orb} > 10^4$ days are soft and are destroyed. *Gaia* DR4 will possibly validate this hypothesis.

4.7. Additional remarks

We have adopted the population-synthesis code SEVN with stellar tracks from PARSEC (Costa et al. 2025). We also reran several models with the MIST tracks (Choi et al. 2016) and found no significant differences. Population-synthesis codes such as SEVN do not model the response of the donor star during mass transfer. This might affect the long-term evolution of a binary system after mass transfer. In a follow-up study, we will run a comparison between our SEVN models and MESA to quantify possible deviations.

Alternative treatments for the transport of angular momentum during non-conservative mass transfer including the possibility that mass is lost via the second Lagrangian point (MacLeod et al. 2018) and the possibility that the excess of angular momentum is redistributed back to the orbit via tides (Paczynski 1991; Popham & Narayan 1991). The latter scenario should lead to results that are qualitatively similar to the Jeans mode for angular momentum transport and widen the orbit rather than shrinking it.

We found that models with stable mass transfer might provide a better description of *Gaia* BH1 and BH2 compared to the α formalism for CE evolution with $\alpha < 1$. This result does not mean that we propose that mass transfer between a $\gtrsim 30$ M$_\odot$ donor and a $\sim 0.5-1.0$ M$_\odot$ accretor is stable. Rather, it confirms that the α formalism does not describe the orbital evolution of a binary system undergoing unstable mass transfer well enough.

Alternative models, such as the γ formalism (Nelemans et al. 2000; Nelemans & Tout 2005) and the recent double-stage CE evolution described by Hirai & Mandel (2022), might provide a final orbital period distribution in between our stable mass-transfer models and the α formalism. For example, Hirai & Mandel (2022) described CE evolution as a dynamically unstable mass-transfer phase until the convective layers of the envelope are ejected, followed by a stable mass-transfer phase when the accretor reaches the deeper radiative layers of the donor. In most cases, this mechanism results in wider final orbital separations than the α formalism.

We considered three models to infer the BH mass from the final properties of the stellar progenitor: the rapid and delayed models from Fryer et al. (2012), and the compactness model based on O'Connor & Ott (2011). These models provide a very approximate description, as the compact-object mass is still largely an open question in core-collapse supernova physics (see, e.g., Burrows & Vartanyan 2021; Maltsev et al. 2025, for a critical discussion of the uncertainties). Hence, our results for the BH mass should be regarded as an approximated phenomenological approach.

5. Summary

We have presented an extensive population-synthesis study of the three *Gaia* BHs with our code SEVN. Our main results are summarized below.

- Natal kicks have a crucial effect on the population of dormant BHs. Kicks modulated by fallback result in a large population of dormant BHs with long orbital periods ($P_{\rm orb} > 10^4$ days) and relatively high BH masses (> 12 M$_\odot$). *Gaia* DR4 will probe the existence of these long orbital period systems, providing constraints on the natal kicks of BHs.
- Models in which the first mass-transfer episode (the episode in which the BH progenitor fills its Roche lobe) is stable, highly non-conservative ($f_{\rm a} \sim 0$), and the angular momentum is lost as a wind from the donor surface (Jeans mode) overall maximize the probability of forming *Gaia* BH-like systems (Table A.1) in terms of orbital period and eccentricity, because these assumptions prevent the initial orbit from shrinking too much. This is a common feature for the three *Gaia* BHs discovered to date.
- Requesting that mass transfer is always stable instead of allowing the onset of CE evolution helps us to produce systems with the orbital periods of *Gaia* BH1 and BH2 especially but not only when combined with strong natal kicks (DM25).
- The high eccentricity of the three *Gaia* BHs is hard to match, unless we assume relatively strong natal kicks (DM25), almost zero accretion efficiency, and the Jeans mode for angular momentum transport.
- When we allowed for CE evolution described with the traditional α formalism, values of $\alpha < 1$ were unable to produce dormant systems similar to the observed *Gaia* BHs. In contrast, values of $\alpha \geq 1$ (together with DM25 kicks) yield qualitatively similar results to our runs with stable mass transfer, low accretion efficiency ($f_{\rm a} = 0$), and the Jeans mode for angular momentum loss. This result confirms that the traditional description of a CE phase (with $\alpha < 1$) provides a poor representation of the orbital evolution of the progenitors of dormant BHs.
- At near solar metallicity, the mass function of dormant BHs peaks at $8 - 10$ M$_\odot$ when we assume the rapid CCSN model. In contrast, the delayed CCSN model and a model based on the compactness criterion tend to produce many more systems with lower-mass BHs (3–8 M$_\odot$) in the orbital period and eccentricity regime of *Gaia* BH1 and BH2.
- According to a simple estimate, our models result in a detection rate of $O(10 - 100)$ dormant BHs in *Gaia* DR3. Models in which natal kicks are weak result in the highest detection rates and might already be in contrast to *Gaia* DR3. We will perform more detailed studies in a follow-up paper.

Our results show that *Gaia* systems might provide key constraints on the formation channels of BHs, complementary to gravitational-wave data. Scenarios with weak natal kicks (e.g., modulated by fallback) for BHs will be likely rejected if *Gaia* DR4 does not include a population of long orbital period systems. Moreover, the efficiency of mass transfer and the mechanism of angular momentum transport during mass transfer also play a key role in shaping the orbital properties of *Gaia* BHs. A major question is the description of the orbital evolution during unstable mass transfer, as our models confirm that the α formalism is a poor description of the process. In future work, we will extend our analysis to include dynamical interactions in star clusters, which drastically increase the parameter space and add further challenges to the numerical modeling of dormant compact objects.

Data availability

SEVN (Iorio et al. 2023) is available via GitLab following this link. Here, we have used version V2.16 (commit 27d4c4e). FIGARO (Rinaldi & Del Pozzo 2024) is publicly available at this link and via `pip`. The main simulation outputs used in this paper and several additional figures are available in Zenodo at this link.

Acknowledgements. We thank Hans-Walter Rix for useful discussions. We acknowledge support from the Deutsche Forschungsgemeinschaft (DFG, German Research Foundation) through project number 546850815 (acronym: DoBlack) and under Germany's Excellence Strategy EXC 2181/1 - 390900948 (the Heidelberg STRUCTURES Excellence Cluster). JMH acknowledges support from the European Research Council for the ERC Advanced Grant [101054731]. CS acknowledges financial support from the Alexander von Humboldt Foundation for the Humboldt Research Fellowship. GI is supported by a fellowship grant from la Caixa Foundation (ID 100010434). The fellowship code is LCF/BQ/PI24/12040020. The simulations were performed thanks to the support of the state of Baden-Württemberg through bwHPC and the DFG through grants INST 35/1597-1 FUGG and INST 35/1503-1 FUGG. This research made use of `cogsworth` and its dependencies (Wagg et al. 2025a,b; Breivik et al. 2020; Price-Whelan 2017). The `cogsworth` population used a star formation history model based on the following papers (Wagg et al. 2022; Frankel et al. 2018; Bovy et al. 2016, 2019; McMillan 2011). Population observables were estimated using dust maps and MIST isochrones (Dotter 2016; Choi et al. 2016; Paxton et al. 2011, 2013, 2015, 2018; Green et al. 2019). This research made use of NumPy (Harris et al. 2020), SciPy (Virtanen et al. 2020), Pandas (The pandas development Team 2024). Plots were produced using Matplotlib (Hunter 2007).

References

Abac, A. G., Abouelfettouh, I., Acernese, F., et al. 2025a, arXiv e-prints, arXiv:2508.18082
Abac, A. G., Abouelfettouh, I., Acernese, F., et al. 2025b, arXiv e-prints, arXiv:2508.18083
Abbott, B. P., Abbott, R., Abbott, T. D., et al. 2016, Phys. Rev. Lett., 116, 061102
Atri, P., Miller-Jones, J. C. A., Bahramian, A., et al. 2019, MNRAS, 489, 3116
Balbinot, E., Dodd, E., Matsuno, T., et al. 2024, A&A, 687, L3
Belczynski, K., Bulik, T., Fryer, C. L., et al. 2010, ApJ, 714, 1217

Bland-Hawthorn, J. & Gerhard, O. 2016, ARA&A, 54, 529
Boco, L., Mapelli, M., Sander, A. A. C., et al. 2025, A&A, 703, A243
Bodensteiner, J., Heida, M., Abdul-Masih, M., et al. 2022, The Messenger, 186, 3
Boesky, A. P., Broekgaarden, F. S., & Berger, E. 2024, ApJ, 976, 24
Bovy, J., Leung, H. W., Hunt, J. A. S., et al. 2019, MNRAS, 490, 4740
Bovy, J., Rix, H.-W., Schlafly, E. F., et al. 2016, ApJ, 823, 30
Breivik, K., Chatterjee, S., & Larson, S. L. 2017, ApJ, 850, L13
Breivik, K., Coughlin, S., Zevin, M., et al. 2020, ApJ, 898, 71
Bressan, A., Marigo, P., Girardi, L., et al. 2012, MNRAS, 427, 127
Burrows, A. & Vartanyan, D. 2021, Nature, 589, 29
Chakrabarti, S., Simon, J. D., Craig, P. A., et al. 2023, AJ, 166, 6
Chattopadhyay, D., Rocha, K. A., Gossage, S., et al. 2026, ApJ, 1000, 190
Chawla, C., Chatterjee, S., & Breivik, K. 2025, arXiv e-prints, arXiv:2508.21805
Chawla, C., Chatterjee, S., Breivik, K., et al. 2022, ApJ, 931, 107
Chen, Y., Bressan, A., Girardi, L., et al. 2015, MNRAS, 452, 1068
Choi, J., Dotter, A., Conroy, C., et al. 2016, ApJ, 823, 102
Costa, G., Shepherd, K. G., Bressan, A., et al. 2025, A&A, 694, A193
Di Carlo, U. N., Agrawal, P., Rodriguez, C. L., & Breivik, K. 2024, ApJ, 965, 22
Di Carlo, U. N., Mapelli, M., Giacobbo, N., et al. 2020, MNRAS, 498, 495
Disberg, P. & Mandel, I. 2025, ApJ, 989, L8
Dotter, A. 2016, ApJS, 222, 8
El-Badry, K. 2024a, New A Rev., 98, 101694
El-Badry, K. 2024b, The Open Journal of Astrophysics, 7, 38
El-Badry, K. & Burdge, K. B. 2022, MNRAS, 511, 24
El-Badry, K., Rix, H.-W., Cendes, Y., et al. 2023a, MNRAS, 521, 4323
El-Badry, K., Rix, H.-W., Latham, D. W., et al. 2024, The Open Journal of Astrophysics, 7, 58
El-Badry, K., Rix, H.-W., Quataert, E., et al. 2023b, MNRAS, 518, 1057
Fantoccoli, F., Barber, J., Dosopoulou, F., Chattopadhyay, D., & Antonini, F. 2025, MNRAS, 538, 243
Farr, W. M., Sravan, N., Cantrell, A., et al. 2011, ApJ, 741, 103
Fragos, T., Andrews, J. J., Ramirez-Ruiz, E., et al. 2019, ApJ, 883, L45
Fragos, T., Willems, B., Kalogera, V., et al. 2009, ApJ, 697, 1057
Frankel, N., Rix, H.-W., Ting, Y.-S., Ness, M., & Hogg, D. W. 2018, ApJ, 865, 96
Fryer, C. L., Belczynski, K., Wiktorowicz, G., et al. 2012, ApJ, 749, 91
Gaia Collaboration, Panuzzo, P., Mazeh, T., et al. 2024, A&A, 686, L2
Ge, H., Webbink, R. F., Chen, X., & Han, Z. 2015, ApJ, 812, 40
Ge, H., Webbink, R. F., Chen, X., & Han, Z. 2020, ApJ, 899, 132
Generozov, A. & Perets, H. B. 2024, ApJ, 964, 83
Giacobbo, N. & Mapelli, M. 2018, MNRAS, 480, 2011
Giesers, B., Dreizler, S., Husser, T.-O., et al. 2018, MNRAS, 475, L15
Giesers, B., Kamann, S., Dreizler, S., et al. 2019, A&A, 632, A3
Gilkis, A. & Mazeh, T. 2024, MNRAS, 535, L44
Gräfener, G. & Hamann, W.-R. 2008, A&A, 482, 945
Green, G. M., Schlafly, E., Zucker, C., Speagle, J. S., & Finkbeiner, D. 2019, ApJ, 887, 93
Halbwachs, J.-L., Pourbaix, D., Arenou, F., et al. 2023, A&A, 674, A9
Harris, C. R., Millman, K. J., van der Walt, S. J., et al. 2020, Nature, 585, 357
Hayashi, T., Suto, Y., & Trani, A. A. 2023, ApJ, 958, 26
Heggie, D. C. 1975, MNRAS, 173, 729
Hills, J. G. & Fullerton, L. W. 1980, AJ, 85, 1281
Hirai, R. & Mandel, I. 2022, ApJ, 937, L42
Hobbs, G., Lorimer, D. R., Lyne, A. G., & Kramer, M. 2005, MNRAS, 360, 974
Hunter, J. D. 2007, Computing in Science and Engineering, 9, 90
Hurley, J. R., Pols, O. R., & Tout, C. A. 2000, MNRAS, 315, 543
Hurley, J. R., Tout, C. A., & Pols, O. R. 2002, MNRAS, 329, 897
Iorio, G., Mapelli, M., Costa, G., et al. 2023, MNRAS, 524, 426
Iorio, G., Torniamenti, S., Mapelli, M., et al. 2024, A&A, 690, A144
Ivanova, N., Justham, S., Chen, X., et al. 2013, A&A Rev., 21, 59
Jayasinghe, T., Stanek, K. Z., Thompson, T. A., et al. 2021, MNRAS, 504, 2577
Kotko, I., Banerjee, S., & Belczynski, K. 2024, MNRAS, 535, 3577
Kroupa, P. 2001, MNRAS, 322, 231
Kruckow, M. U., Andrews, J. J., Fragos, T., et al. 2024, A&A, 692, A141
Lada, C. J. & Lada, E. A. 2003, ARA&A, 41, 57
Li, Z., Lu, X., Lü, G., et al. 2026a, A&A, 706, A105
Li, Z., Wei, D., Jia, S., et al. 2026b, ApJ, 1004, 31
Li, Z., Zhu, C., Lu, X., et al. 2024, ApJ, 975, L8
Licquia, T. C. & Newman, J. A. 2015, ApJ, 806, 96
MacLeod, M., Ostriker, E. C., & Stone, J. M. 2018, ApJ, 863, 5
Mahy, L., Sana, H., Shenar, T., et al. 2022, A&A, 664, A159
Maltsev, K., Schneider, F. R. N., Mandel, I., et al. 2025, A&A, 700, A20
Mapelli, M., Colpi, M., & Zampieri, L. 2009, MNRAS, 395, L71
Mapelli, M. & Giacobbo, N. 2018, MNRAS, 479, 4391
Mapelli, M., Spera, M., Montanari, E., et al. 2020, ApJ, 888, 76
Marín Pina, D., Gieles, M., Rastello, S., et al. 2026, arXiv e-prints, arXiv:2604.24874
Marín Pina, D., Rastello, S., Gieles, M., et al. 2024, A&A, 688, L2
McMillan, P. J. 2011, MNRAS, 414, 2446
Moe, M. & Di Stefano, R. 2017, ApJS, 230, 15
Müller-Horn, J., Ramachandran, V., El-Badry, K., et al. 2026, A&A, 708, A187
Nagarajan, P. & El-Badry, K. 2025, PASP, 137, 034203
Nagarajan, P., El-Badry, K., Chawla, C., et al. 2025, PASP, 137, 044202
Nelemans, G. & Tout, C. A. 2005, MNRAS, 356, 753
Nelemans, G., Verbunt, F., Yungelson, L. R., & Portegies Zwart, S. F. 2000, A&A, 360, 1011
Nguyen, C. T., Costa, G., Bressan, A., et al. 2025, A&A, 701, A258
O'Connor, E. & Ott, C. D. 2011, ApJ, 730, 70
Olejak, A., Klencki, J., Vigna-Gomez, A., et al. 2025, arXiv e-prints, arXiv:2511.10728
Özel, F., Psaltis, D., Narayan, R., & McClintock, J. E. 2010, ApJ, 725, 1918
Paczynski, B. 1991, ApJ, 370, 597
Paczyński, B. & Ziółkowski, J. 1968, Acta Astron., 18, 255
Pauli, D., Langer, N., Schootemeijer, A., et al. 2026, A&A, 707, A11

Paxton, B., Bildsten, L., Dotter, A., et al. 2011, ApJS, 192, 3
Paxton, B., Cantiello, M., Arras, P., et al. 2013, ApJS, 208, 4
Paxton, B., Marchant, P., Schwab, J., et al. 2015, ApJS, 220, 15
Paxton, B., Schwab, J., Bauer, E. B., et al. 2018, ApJS, 234, 34
Popham, R. & Narayan, R. 1991, ApJ, 370, 604
Price-Whelan, A. M. 2017, The Journal of Open Source Software, 2
Rastello, S., Iorio, G., Mapelli, M., et al. 2023, MNRAS, 526, 740
Repetto, S., Igoshev, A. P., & Nelemans, G. 2017, MNRAS, 467, 298
Rinaldi, S. & Del Pozzo, W. 2024, The Journal of Open Source Software, 9, 6589
Romagnolo, A., Broekgaarden, F. S., Antoniadis, K., & Gormaz-Matamala, A. C. 2026, arXiv e-prints, arXiv:2601.02263
Röpke, F. K. & De Marco, O. 2023, Living Reviews in Computational Astrophysics, 9, 2
Sabhahit, G. N., Vink, J. S., Sander, A. A. C., & Higgins, E. R. 2023, MNRAS, 524, 1529
Sana, H., de Mink, S. E., de Koter, A., et al. 2012, Science, 337, 444
Saracino, S., Kamann, S., Guarcello, M. G., et al. 2022, MNRAS, 511, 2914
Saracino, S., Shenar, T., Kamann, S., et al. 2023, MNRAS, 521, 3162
Sgalletta, C., Mapelli, M., Boco, L., et al. 2025, A&A, 698, A144
Shahaf, S., Bashi, D., Mazeh, T., et al. 2023, MNRAS, 518, 2991
Shenar, T., Sana, H., Mahy, L., et al. 2022, Nature Astronomy, 6, 1085
Shikauchi, M., Kumamoto, J., Tanikawa, A., & Fujii, M. S. 2020, PASJ, 72, 45
Shikauchi, M., Tanikawa, A., & Kawanaka, N. 2022, ApJ, 928, 13
Shikauchi, M., Tsuna, D., Tanikawa, A., & Kawanaka, N. 2023, ApJ, 953, 52
Spera, M. & Mapelli, M. 2017, MNRAS, 470, 4739
Spera, M., Mapelli, M., Giacobbo, N., et al. 2019, MNRAS, 485, 889
Tanikawa, A., Cary, S., Shikauchi, M., Wang, L., & Fujii, M. S. 2024a, MNRAS, 527, 4031
Tanikawa, A., Hattori, K., Kawanaka, N., et al. 2023, ApJ, 946, 79
Tanikawa, A., Wang, L., & Fujii, M. S. 2024b, The Open Journal of Astrophysics, 7, 39
The pandas development Team. 2024, pandas-dev/pandas: Pandas
Thompson, T. A., Kochanek, C. S., Stanek, K. Z., et al. 2019, Science, 366, 637
Trimble, V. L. & Thorne, K. S. 1969, ApJ, 156, 1013
Vinciguerra, S., Neijssel, C. J., Vigna-Gómez, A., et al. 2020, MNRAS, 498, 4705
Virtanen, P., Gommers, R., Oliphant, T. E., et al. 2020, Nature Methods, 17, 261
Wagg, T., Breivik, K., Renzo, M., & Price-Whelan, A. 2025a, The Journal of Open Source Software, 10, 7400
Wagg, T., Breivik, K., Renzo, M., & Price-Whelan, A. M. 2025b, ApJS, 276, 16
Wagg, T., Broekgaarden, F. S., de Mink, S. E., et al. 2022, ApJ, 937, 118
Wiktorowicz, G., Lu, Y., Wyrzykowski, Ł., et al. 2020, ApJ, 905, 134
Willcox, R., Marchant, P., Vigna-Gómez, A., et al. 2025, A&A, 700, A59
Woosley, S. E., Heger, A., & Weaver, T. A. 2002, Reviews of Modern Physics, 74, 1015
Yamaguchi, N., El-Badry, K., & Shahaf, S. 2025, PASP, 137, 104205
Zak, J., Jones, D., Boffin, H. M. J., et al. 2023, MNRAS, 524, 5749
Zeldovich, Y. B. & Guseynov, O. H. 1966, ApJ, 144, 840
Zevin, M., Spera, M., Berry, C. P. L., & Kalogera, V. 2020, ApJ, 899, L1
Zorotovic, M., Schreiber, M. R., & Gänsicke, B. T. 2011, A&A, 536, A42

Appendix A: Summary of the models presented in the main text

Table A.1 summarizes the models presented in the main text (i.e., with CE parameter $\alpha = 1$ or stable mass transfer).

Appendix B: CE evolution and efficiency parameter

In the runs where CE evolution is allowed, we assume that mass transfer is unstable when the mass ratio q between donor and accretor exceeds the list of critical values q_c indicated in Table B.1.

In the main text, we assume that CE evolution is described with efficiency parameter $\alpha = 1$. Here, we show models with CE ejection efficiency parameter $\alpha \neq 1$. Table B.2 summarizes the models we considered with $\alpha = 0.1$, 0.5, 2, 3, 5, 7, 10, and 15. Figures B.1, B.2, B.3, B.4, and B.5 show the main properties of models with $\alpha = 0.1$, 0.5, 2, 5, and 15. The figures clearly show that the orbital period distribution of dormant BHs shifts to large values with increasing α. This happens because higher values of α imply that less orbital energy is requested to eject the CE; hence the orbital separation shrinks less. The same trend can be seen in both models with isotropic re-emission and $f_a = 0.5$ and models with Jeans mode and $f_a = 0.0$.

Overall, the properties of Gaia BH1 can be matched by models with $\alpha \in [1, 7]$, as shown by the figures and by the percentile analysis in Table B.2.

Table B.2 also shows that the efficiency of compact-object binary formation is maximum for small values of α and minimum for larger values. This happens because small values of α shrink more efficiently the orbit during CE evolution, thus allowing more systems to remain bound during the CCSN explosion. Some of the systems with the shorter orbital separations (less than a few days) might be observable as X-ray binary systems, but here we do not introduce any emission models to distinguish dormant and X-ray active systems. We will investigate this aspect in a follow-up work. Systems matching the properties of *Gaia* BH1, BH2, and BH3 are not Roche-lobe filling, thus they do not require that we make a detailed distinction between dormant and X-ray active systems for the purpose of this work.

Appendix C: Thermal eccentricity distribution

In this section we report the results of a subset of runs performed assuming a thermal distribution $\mathcal{F}(e) \propto e$ for the initial orbital eccentricities. Models in which the natal kicks are modulated by fallback show two main differences. Firstly and most importantly, the long orbital period systems that survive bound until they become *Gaia* BH-like systems tend to have higher eccentricities (Fig. C.1). Indeed, these systems do not undergo Roche-lobe overflow and their final eccentricities retain memory of the initial distribution. Secondly, a slightly larger number of systems are disrupted by natal kicks, because of the larger eccentricity. The difference is by a factor of ≈ 1.3 and it is visible by comparing the formation efficiency $\eta_{\rm dorm}$ in Table C.1 with the values in Table A.1.

In contrast, when DM25 natal kicks are assumed (Fig. C.2), there is negligible difference between a thermal and a Sana et al. (2012) initial eccentricity distribution. This is because the long orbital period systems are disrupted by natal kicks, whereas the short orbital period systems interact via Roche-lobe overflow and circularize before the natal kick: the final evolution of these systems is completely determined by mass transfer and natal kicks.

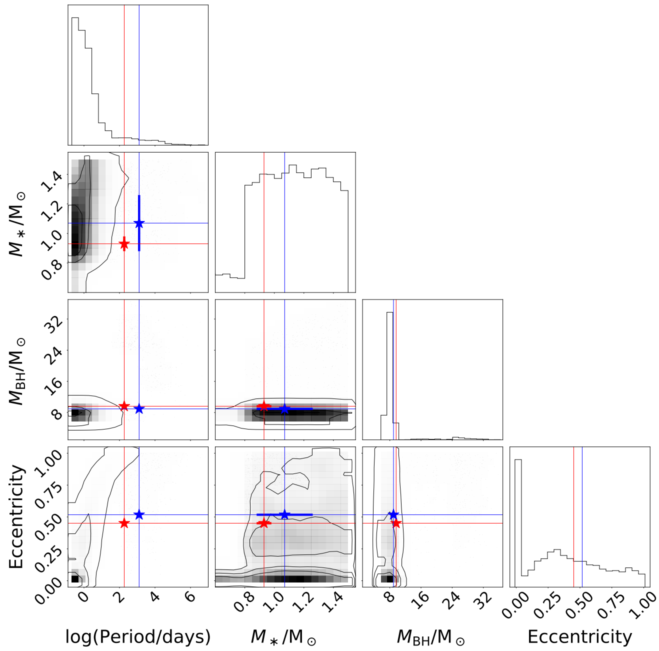

Fig. B.1. Corner plot showing the orbital period, eccentricity, BH mass ($M_{\rm BH}$) and companion star mass (M_*) in the simulations of model $A_{\alpha01}$ with $\alpha = 0.1$. The red and blue stars show the values for *Gaia* BH1 and BH2.

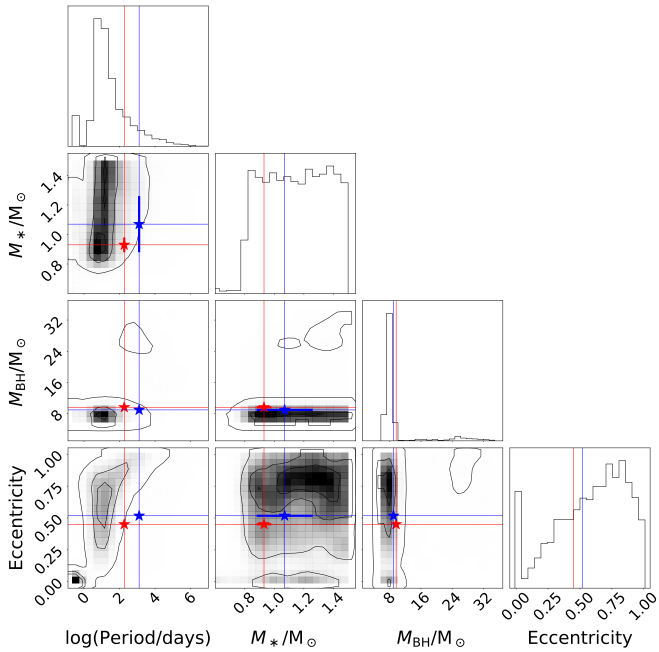

Fig. B.2. Same as Fig. B.1 but for model $A_{\alpha05}$ with $\alpha = 0.5$.

Appendix D: Mock observations

To construct the mock observations, we matched each simulated dormant BH binary to a synthetic Milky Way stellar population generated with the python package `cogsworth` (Wagg et al. 2025b). Each binary was assigned to a randomly sampled star with the same luminous companion mass, adopting its 3D Galactocentric position. We generated the `cogsworth` population using the default Milky Way parameters and solar metallicity. We

Table A.1. Models presented in the main text (with CE parameter α = 1 or stable mass transfer).

Model	CE	α	CCSN	Fallback	f_a	Ang. Mom.	Z	Perc. BH1	Perc. BH2	Perc. BH3	$\eta_{\rm dorm}$ [$\times 10^{-7}$ M$_\odot{}^{-1}$]
A	Y	1	R	N	0.5	Isot	0.014	$99.69^{+0.26}_{-5.78}$	$99.95^{+0.01}_{-0.01}$	$99.95^{+0.01}_{-0.07}$	8.3
Afb	Y	1	R	Y	0.5	Isot	0.014	$96.54^{+3.20}_{-10.98}$	$99.78^{+0.22}_{-0.37}$	$99.74^{+0.17}_{-0.79}$	467.4
	Y	1	R	N	0.0	Isot.	0.014	$99.75^{+0.20}_{-2.56}$	$99.95^{+0.01}_{-0.01}$	$99.95^{+0.01}_{-0.52}$	8.5
	Y	1	R	Y	0.0	Isot.	0.014	$98.95^{+0.97}_{-4.54}$	$99.90^{+0.10}_{-0.17}$	$99.81^{+0.16}_{-0.90}$	467.3
AJ	Y	1	R	N	0.0	Jeans	0.014	$99.64^{+0.31}_{-5.51}$	$99.95^{+0.01}_{-0.01}$	$99.95^{+0.01}_{-0.01}$	8.3
AJfb	Y	1	R	Y	0.0	Jeans	0.014	$95.76^{+3.85}_{-3.65}$	$99.76^{+0.24}_{-1.05}$	$99.58^{+0.35}_{-0.75}$	467.3
	Y	1	R	N	1.0	Isot	0.014	$99.75^{+0.20}_{-2.31}$	$99.95^{+0.01}_{-0.10}$	$99.92^{+0.03}_{-0.73}$	8.6
	Y	1	R	Y	1.0	Isot	0.014	$96.29^{+3.57}_{-6.02}$	$99.92^{+0.08}_{-0.30}$	$99.50^{+0.39}_{-0.83}$	467.1
	Y	1	R	N	0.5	Isot	0.017	$97.92^{+1.99}_{-9.36}$	$99.92^{+0.01}_{-0.01}$	$99.92^{+0.01}_{-0.01}$	5.2
	Y	1	R	N	0.0	Jeans	0.017	$96.41^{+3.51}_{-10.91}$	$99.91^{+0.01}_{-0.01}$	$99.91^{+0.01}_{-0.01}$	4.9
AlowZ	Y	1	R	N	0.5	Isot	1.4×10^{-4}	$99.96^{+0.01}_{-0.01}$	$99.81^{+0.15}_{-18.76}$	$98.19^{+1.77}_{-36.93}$	11.2
AJlowZ	Y	1	R	N	0.0	Jeans	1.4×10^{-4}	$99.96^{+0.01}_{-0.04}$	$99.96^{+0.01}_{-0.84}$	$99.90^{+0.06}_{-19.83}$	10.4
B	N	–	R	N	0.5	Isot.	0.014	$99.86^{+0.01}_{-0.01}$	$99.86^{+0.01}_{-0.01}$	$99.86^{+0.01}_{-2.75}$	3.05
Bfb	N	–	R	Y	0.5	Isot.	0.014	$99.98^{+0.01}_{-0.01}$	$99.98^{+0.02}_{-0.06}$	$99.93^{+0.06}_{-1.0}$	459.2
	N	–	R	N	0.0	Isot.	0.014	$99.98^{+0.01}_{-0.015}$	$99.98^{+0.02}_{-0.20}$	$99.98^{+0.01}_{-0.97}$	27.9
	N	–	R	Y	0.0	Isot.	0.014	$99.94^{+0.02}_{-0.03}$	$99.95^{+0.05}_{-0.06}$	$99.27^{+0.54}_{-1.17}$	488.7
BJ	N	–	R	N	0.0	Jeans	0.014	$\mathbf{86.39^{+13.59}_{-29.16}}$	$\mathbf{88.06^{+11.92}_{-24.08}}$	$99.98^{+0.01}_{-0.13}$	22.7
BJfb	N	–	R	Y	0.0	Jeans	0.014	$\mathbf{83.58^{+10.51}_{-12.69}}$	$\mathbf{88.63^{+11.37}_{-10.59}}$	$99.57^{+0.38}_{-1.18}$	743.0
	N	–	R	N	0.0	Jeans	0.017	$91.29^{+8.69}_{-27.46}$	$92.85^{+7.12}_{-19.49}$	$99.98^{+0.01}_{-0.01}$	17.8
	N	–	R	N	0.0	Jeans	1.4×10^{-4}	$96.84^{+3.02}_{-5.11}$	$98.99^{+1.00}_{-4.24}$	$96.14^{+3.69}_{-4.10}$	252.1
C	Y	1	C	N	0.5	Isot.	0.014	$99.27^{+0.53}_{-0.48}$	$99.97^{+0.02}_{-0.07}$	$99.99^{+0.01}_{-0.38}$	47.2
	Y	1	C	Y	0.5	Isot	0.014	$99.99^{+0.01}_{-0.018}$	$99.99^{+0.01}_{0.01}$	$99.97^{+0.03}_{-0.48}$	1267.7
	N	–	C	N	0.5	Isot	0.014	$99.98^{+0.01}_{-0.01}$	$99.98^{+0.01}_{-0.08}$	$99.98^{+0.01}_{-0.18}$	22.7
	N	–	C	Y	0.5	Isot	0.014	$99.92^{+0.05}_{-0.03}$	$99.88^{+0.12}_{-0.14}$	$99.95^{+0.05}_{-1.08}$	1164.3
D	Y	1	D	N	0.5	Isot.	0.014	$99.96^{+0.01}_{-4.36}$	$99.96^{+0.01}_{-0.01}$	$99.96^{+0.01}_{-0.71}$	11.0
	Y	1	D	Y	0.5	Isot.	0.014	$96.53^{+3.11}_{-5.88}$	$99.76^{+0.24}_{-0.32}$	$99.63^{+0.34}_{-1.70}$	382.5
	Y	1	D	N	0.0	Isot.	0.014	$99.96^{+0.01}_{-0.44}$	$99.96^{+0.01}_{-0.01}$	$99.88^{+0.08}_{-0.28}$	10.9
	Y	1	D	Y	0.0	Isot.	0.014	$97.77^{+2.08}_{-11.38}$	$99.84^{+0.16}_{-0.40}$	$99.77^{+0.20}_{-1.15}$	382.9
	Y	1	D	N	0.0	Jeans	0.014	$99.90^{+0.06}_{-4.82}$	$99.96^{+0.01}_{-0.01}$	$99.96^{+0.01}_{-0.74}$	10.8
	Y	1	D	Y	0.0	Jeans	0.014	$96.54^{+3.29}_{-8.32}$	$99.59^{+0.41}_{-0.30}$	$99.92^{+0.06}_{-0.14}$	382.9
	Y	1	D	N	1.0	Isot	0.014	$99.96^{+0.01}_{-1.94}$	$99.96^{+0.01}_{-0.01}$	$99.96^{+0.01}_{-0.75}$	6.69
	Y	1	D	Y	1.0	Isot	0.014	$97.42^{+2.20}_{-6.64}$	$99.74^{+0.26}_{-0.25}$	$99.93^{+0.06}_{-1.08}$	383.0
	Y	1	D	N	0.5	Isot.	0.017	$99.75^{+0.18}_{-7.88}$	$99.93^{+0.01}_{-0.01}$	$99.93^{+0.01}_{-0.01}$	6.1
	Y	1	D	N	0.5	Isot	1.4×10^{-4}	$99.96^{+0.01}_{-2.81}$	$97.92^{+2.04}_{-21.77}$	$97.02^{+2.94}_{-23.28}$	10.5
	N	–	D	N	0.5	Isot.	0.014	$99.87^{+0.02}_{-0.015}$	$99.80^{+0.19}_{-0.49}$	$99.68^{+0.20}_{-0.62}$	84.3
	N	–	D	Y	0.5	Isot.	0.014	$99.92^{+0.01}_{-0.02}$	$99.90^{+0.10}_{-0.05}$	$99.86^{+0.05}_{-0.35}$	472.0
	N	–	D	N	0.0	Isot.	0.014	$99.94^{+0.05}_{-0.04}$	$99.89^{+0.093}_{-0.33}$	$99.85^{+0.14}_{-0.54}$	34.9
	N	–	D	Y	0.0	Isot.	0.014	$99.89^{+0.08}_{-0.09}$	$99.88^{+0.12}_{-0.12}$	$99.83^{+0.12}_{-0.19}$	415.1
	N	–	D	N	0.0	Jeans	0.014	$\mathbf{69.33^{+30.55}_{-31.19}}$	$92.74^{7.23}_{-25.44}$	$99.98^{+0.02}_{-0.06}$	21.4
	N	–	D	Y	0.0	Jeans	0.014	$\mathbf{80.27^{+17.94}_{-8.75}}$	$\mathbf{88.19^{+11.80}_{-17.31}}$	$99.61^{+0.31}_{-1.61}$	533.6
	N	–	D	N	1.0	Isot.	0.014	$99.86^{+0.06}_{-0.06}$	$99.96^{+0.04}_{-0.10}$	$99.93^{+0.04}_{-0.15}$	122.7
	N	–	D	Y	1.0	Isot.	0.014	$99.91^{+0.02}_{-0.07}$	$99.91^{+0.08}_{-0.12}$	$99.78^{+0.13}_{-0.50}$	527.1
	N	–	D	N	0.5	Isot.	0.017	$99.92^{+0.03}_{-0.07}$	$99.62^{+0.38}_{-0.95}$	$99.97^{+0.02}_{-0.02}$	73.3
	N	–	D	N	0.5	Isot	1.4×10^{-4}	$\mathbf{78.56^{+20.36}_{-23.59}}$	$94.60^{+5.40}_{-19.68}$	$97.58^{+2.41}_{-26.37}$	70.8

Column 1: Model name (only the main models discussed in the text and in the figures have a name for faster reference); Col. 2: Y (N) means that the α formalism for CE evolution is (is not) activated; Col. 3: value of the CE α parameter; Col. 4: CCSN model – R for rapid, D for delayed, C for compactness criterion; Col. 5: the natal kick is modulated by fallback (Y) or not (N); Col. 6: accretion efficiency (f_a); Col. 7: angular momentum transport mode (isotropic re-emission or Jeans mode); Col. 8: metallicity Z; Cols. 8-10: percentile value of *Gaia* BH1, BH2, and BH3 (median values and 68% credible intervals); Col. 11: formation efficiency $\eta_{\rm dorm}$ of BH binaries with a 0.5–1.5 M$_\odot$ stellar companion (Eq. 3).

Table B.1. Adopted q_c values.

Evolutionary Stage of the Donor	q_c
Main Sequence	3.0
Hertzsprung Gap	4.0
First Giant Branch	Eq. 57, Hurley et al. (2002)
Core He Burning	3.0
Asymptotic Giant Branch	Eq. 57, Hurley et al. (2002)
He Main Sequence	3.0
He Hertzsprung Gap	0.784
He Giant Branch	0.784
White Dwarf	0.628
Neutron Star/Black Hole	Merger

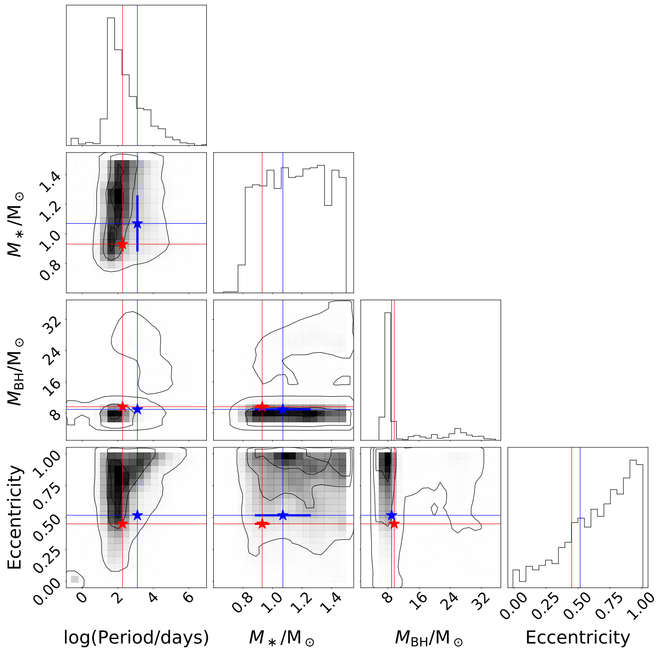

Fig. B.3. Same as Fig. B.1 but for model $A_{\alpha 2}$ with α = 2.

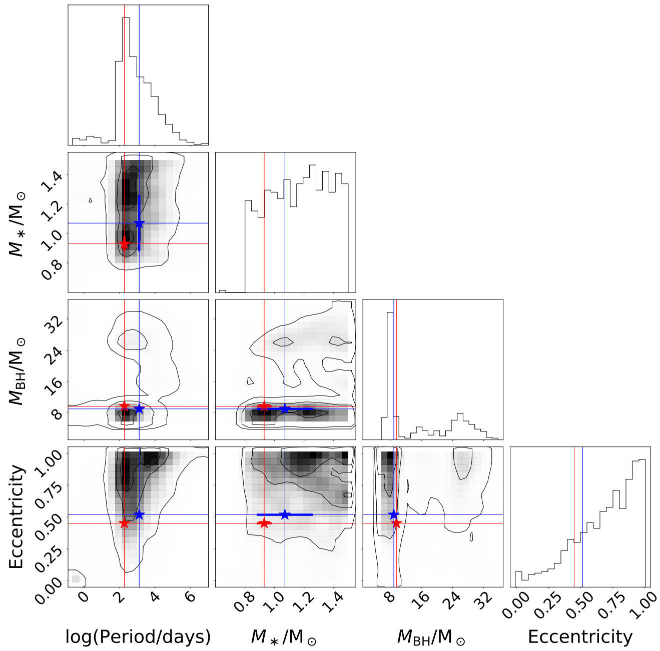

Fig. B.4. Same as Fig. B.1 but for model $A_{\alpha 5}$ with α = 5.

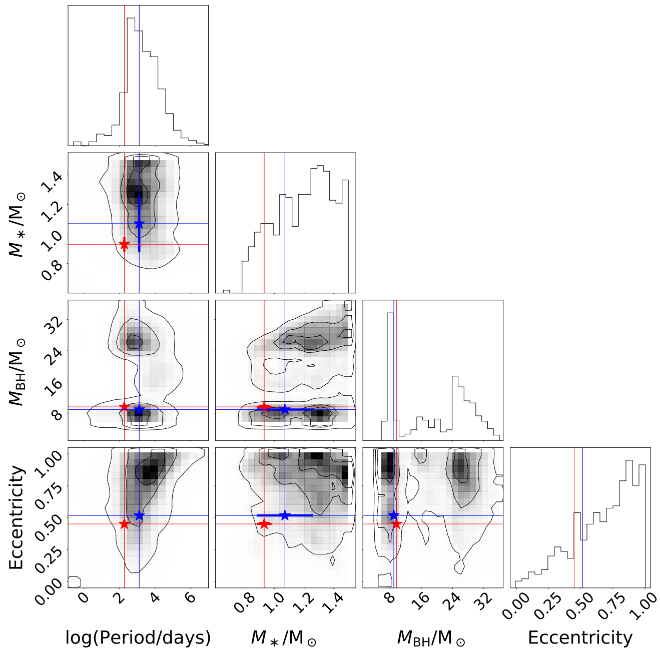

Fig. B.5. Same as Fig. B.1 but for model $A_{\alpha 15}$ with α = 15.

sampled only single stars, as we have already simulated binary interactions with SEVN. To improve computational efficiency, we proceeded in two steps. First, we estimated the probability that a system lies within an effective search volume of 10 kpc, beyond which the astrometric signal is typically too small for detection in *Gaia* DR3. We find that ∼ 60% of the systems fall within this volume. Second, we evaluated the probability of detection for systems within this volume.

Within the 10 kpc volume, we resampled stars from the `cogsworth` population and matched them to the simulated BH binaries by companion mass. We generated 50 realizations per system to increase the statistical robustness. For each realization, we computed observable quantities (sky position, proper motion and distance) with `cogsworth` and simulated extinction and apparent magnitudes in the *Gaia G* band using the Bayestar dust map (Green et al. 2019). We randomly sampled orbital orientations and phases, while intrinsic binary parameters (BH mass, orbital period, and eccentricity) remained fixed to the values simulated with SEVN.

We then processed the mock binaries with the `gaiamock` pipeline (El-Badry 2024a), which simulates *Gaia* epoch astrometry based on the scanning law and empirically calibrated uncertainties. `gaiamock` fits the resulting data with the full astrometric fitting cascade, assigning single-star, acceleration, or orbital solutions following the DR3 data model. We classify systems as detected if they meet the DR3 non-single star quality cuts (Halbwachs et al. 2023) and would have most likely received a 12-parameter orbital solution. We calculated the average detection probability across the population and obtained $p_{\rm det} = 2.9 \times 10^{-4}$ and 8.0×10^{-5} for models A and Afb, respectively (including the factor of 0.6 for the effective search volume).

Table B.2. Models with CE parameter $\alpha \neq 1$.

Model	CE	α	CCSN	Fallback	f_a	Ang. Mom.	Z	Perc. BH1	Perc. BH2	Perc. BH3	$\eta_{\rm dorm}$ [$\times 10^{-7}$ M$_\odot{}^{-1}$]
$A_{\alpha 01}$	Y	0.1	R	N	0.5	Isot	0.014	$99.98^{+0.01}_{-0.01}$	$99.98^{+0.01}_{-0.01}$	$99.95^{+0.03}_{-0.42}$	22.1
$AJ_{\alpha 01}$	Y	0.1	R	N	0.0	Jeans	0.014	$99.98^{+0.01}_{-0.01}$	$99.98^{+0.01}_{-0.01}$	$99.96^{+0.02}_{-0.11}$	21.2
$A_{\alpha 05}$	Y	0.5	R	N	0.5	Isot	0.014	$99.96^{+0.01}_{-0.18}$	$99.96^{+0.01}_{-0.01}$	$99.91^{+0.05}_{-0.60}$	11.9
$AJ_{\alpha 05}$	Y	0.5	R	N	0.0	Jeans	0.014	$99.96^{+0.01}_{-0.01}$	$99.96^{+0.01}_{-0.01}$	$99.96^{+0.01}_{-0.45}$	11.9
$A_{\alpha 2}$	Y	2	R	N	0.5	Isot	0.014	$97.56^{+2.37}_{-23.92}$	$99.93^{+0.01}_{-0.01}$	$99.93^{+0.01}_{-0.01}$	5.8
$AJ_{\alpha 2}$	Y	2	R	N	0.0	Jeans	0.014	$98.30^{+1.55}_{-7.22}$	$99.93^{+0.01}_{-0.01}$	$99.93^{+0.01}_{-0.01}$	5.8
$A_{\alpha 3}$	Y	3	R	N	0.5	Isot	0.014	$97.14^{+2.77}_{-14.65}$	$99.91^{+0.01}_{-0.01}$	$99.91^{+0.01}_{-0.47}$	4.8
$AJ_{\alpha 3}$	Y	3	R	N	0.0	Jeans	0.014	$90.77^{+9.14}_{-26.51}$	$99.86^{+0.05}_{-2.63}$	$99.91^{+0.01}_{-0.66}$	4.7
$A_{\alpha 5}$	Y	5	R	N	0.5	Isot	0.014	$96.26^{+3.51}_{-17.51}$	$98.04^{+1.84}_{-11.64}$	$99.87^{+0.01}_{-1.39}$	3.4
$AJ_{\alpha 5}$	Y	5	R	N	0.0	Jeans	0.014	$96.40^{+3.48}_{-12.98}$	$99.70^{+0.18}_{-13.87}$	$99.88^{+0.01}_{-1.60}$	3.6
$A_{\alpha 7}$	Y	7	R	N	0.5	Isot	0.014	$99.55^{+0.28}_{-14.03}$	$99.82^{+0.0}_{-9.65}$	$99.82^{+0.01}_{-1.80}$	2.4
$AJ_{\alpha 7}$	Y	7	R	N	0.0	Jeans	0.014	$99.30^{+0.53}_{-6.34}$	$99.82^{+0.01}_{-0.70}$	$99.82^{+0.01}_{-0.01}$	2.5
$A_{\alpha 10}$	Y	10	R	N	0.5	Isot	0.014	$98.83^{+1.01}_{-13.17}$	$95.64^{+4.19}_{-28.81}$	$99.83^{+0.01}_{-0.19}$	2.6
$AJ_{\alpha 10}$	Y	10	R	N	0.0	Jeans	0.014	$99.19^{+0.65}_{-6.51}$	$\mathbf{78.18^{+21.66}_{-37.78}}$	$99.84^{+0.01}_{-0.01}$	2.6
$A_{\alpha 15}$	Y	15	R	N	0.5	Isot	0.014	$99.80^{+0.01}_{-0.40}$	$99.80^{+0.01}_{-29.07}$	$99.80^{+0.01}_{-0.23}$	2.2
$AJ_{\alpha 15}$	Y	15	R	N	0.0	Jeans	0.014	$99.81^{+0.01}_{-2.72}$	$99.81^{+0.01}_{-34.78}$	$99.81^{+0.01}_{-0.01}$	2.2

Notes. The description of the columns is the same as in Table A.1.

Table C.1. Models that assume a thermal distribution for the initial orbital eccentricity.

Model	CE	α	CCSN	Fallback	f_a	Ang. Mom.	Z	Perc. BH1	Perc. BH2	Perc. BH3	$\eta_{\rm dorm}$ [$\times 10^{-7}$ M$_\odot{}^{-1}$]
A_th	Y	1	R	N	0.5	Isot	0.014	$99.94^{+0.01}_{-0.26}$	$99.94^{+0.01}_{-0.01}$	$99.94^{+0.01}_{-1.10}$	6.8
Afb_th	Y	1	R	Y	0.5	Isot	0.014	$91.67^{+5.34}_{-2.57}$	$99.20^{+0.80}_{-0.40}$	$99.71^{+0.27}_{-0.97}$	358.5
	Y	1	R	N	0.0	Jeans	0.014	$99.94^{+0.01}_{-0.26}$	$99.94^{+0.01}_{-0.01}$	$99.94^{+0.01}_{-0.01}$	6.7
	Y	1	R	Y	0.0	Jeans	0.014	$95.16^{+3.52}_{-12.41}$	$99.83^{+0.17}_{-0.44}$	$99.73^{+0.26}_{-2.02}$	358.5

Notes. The description of the columns is the same as in Table A.1.

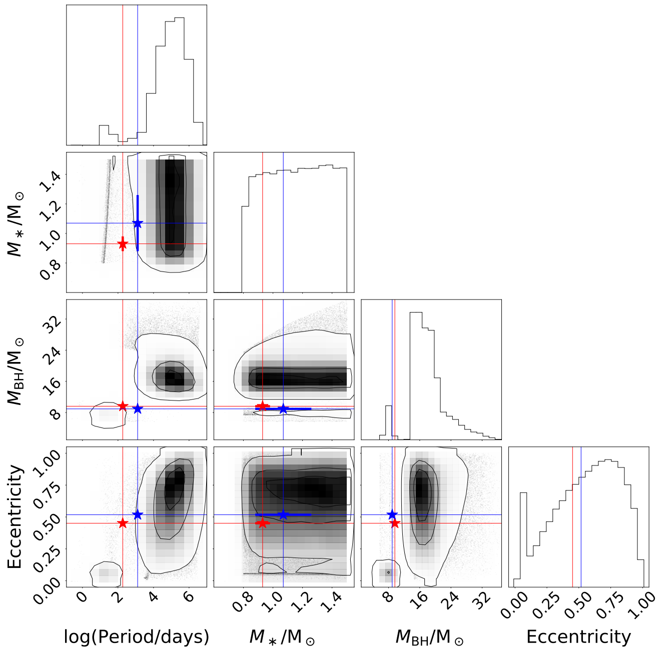

Fig. C.1. Same as Fig. 1 but assuming a thermal distribution $\mathcal{F}(e) \propto e$ for the initial orbital eccentricity.

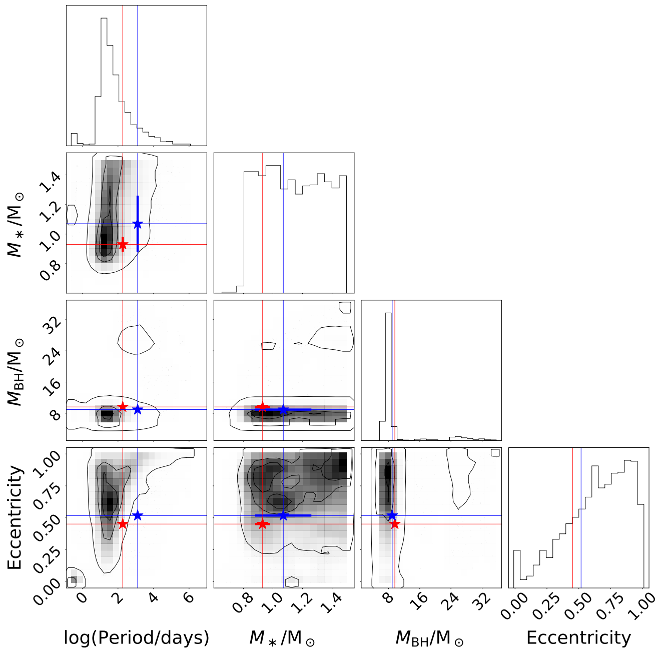

Fig. C.2. Same as Fig. 2 but assuming a thermal distribution $\mathcal{F}(e) \propto e$ for the initial orbital eccentricity.